AN ABSTRACT OF THE THESIS OF

Jeremy C. Conner for the degree of Master of Science in Civil Engineering

presented on May 1, 2013.

Title: Quantification of Landslide Movement in a Forested Environment

Abstract approved:

_____

Michael J. Olsen

Landslides are an insidious natural hazard, which can result in significant damage to public infrastructure. Limited monitoring tools are available, particularly tools suitable for use in forested environments. These tools often only allow a few locations across the slide to be monitored. Terrestrial Laser Scanning (TLS) shows promise as a monitoring technique given the high spatial resolution and accuracy at which measurements can be made. However, current procedures can be time consuming, require advanced skill and judgment by the analyst, and typically require manual methods of feature extraction to quantify landslide movement.

To overcome these limitations, this thesis presents and investigates a new methodology to detect and monitor landslide movement in a densely forested area using natural features such as tree trunks. The presented methodology searches through the noisy point cloud dataset to find trees and

then fit circles to points sampled on the tree trunk. Next, comparing the movement of the circles between time series terrestrial laser scan surveys provides quantified displacements distributed across the landslide. For quality control purposes a parametric analysis was conducted and revealed that the root mean square error (RMS) of the circle fit and the difference in calculated tree radii between epochs are the dominant parameters in correctly pairing trees between epochs. For the test dataset, the optimal values were a RMS circle-fit of less than 1.5 cm and less than 1.0 cm for the calculated difference in tree radii.

Application of the methodology to a case study of Johnson Creek Landslide (JCL) showed that TLS can determine landslide movement comparable to conventional monitoring methods. The displacements observed on markers were within 2 cm from the displacement observed from traditional methods such as total station monitoring. TLS also provides more samples than currently observed for this location, allowing increased detail for landslide modeling and monitoring.

Quantification of Landslide Movement in a Forested Environment

by
Jeremy C. Conner

A THESIS

submitted to

Oregon State University

in partial fulfillment of
the requirements for the
degree of

Master of Science

Presented May 1, 2013
Commencement June 2013

Master of Science thesis of Jeremy C. Conner presented on May 1, 2013.

APPROVED:

_____

Major Professor, representing Civil Engineering

_____

Head of the School of Civil and Construction Engineering

_____

Dean of the Graduate School

I understand that my thesis will become part of the permanent collection of Oregon State University libraries. My signature below authorizes release of my thesis to any reader upon request.

_____

Jeremy C. Conner, Author

ACKNOWLEDGEMENTS

I would first like to thank my wife, Crystal Conner, for her continuous support in everything I do. Also to my children, Sophia and Luke, who are my little troopers that keep me going no matter what the circumstances are.

I want to recognize my committee members Anne Nolin, Daniel Gillins, and Paul Vincent for their time and help in reviewing my thesis. This thesis would not have been possible without the extensive mentorship and assistance provided by Michael Olsen. His guidance started before I ever arrived in Oregon and I am sure it will continue after I leave OSU because that is the type of person he is. Thank you for everything you have provided me over the past two years.

I have to thank the Army and West Point for providing me the opportunity to attend graduate school before returning to West Point as an instructor. Without this opportunity, graduate school would have never been a possibility.

I also want to thank Professor Robert Schultz for providing me the knowledge base to instruct the classes I will teach at West Point upon my arrival.

Thank you to Keith Williams, Rubini Mahalingam, and John Raugust for assistance with data collection and long days at the Oregon coast, and everyone in the Geomatics lab for your help.

Thank you to DOGAMI for a thorough Johnson Creek Landslide site visit physically showing and explaining previous work done and the geological setting.

Finally, thank you to Leica Geosystems, David Evans & Associates, Maptek I-Site, and Oregon Department of Transportation for providing the equipment and software used for this research. Additionally, Oregon Department of Transportation provided travel support for data acquisition.

CONTRIBUTION OF AUTHORS

Dr. Michael Olsen assisted with direction, guidance and editing on all Chapters presented.

Keith Williams, Rubini Mahalingam, and John Raugust assisted with data collection at Johnson Creek Landslide.

Mahyar Sharifi-Mood wrote code to fit one circle to a dataset of points, which was modified to detect multiple trees throughout an entire dataset for analysis of Johnson Creek Landslide.

TABLE OF CONTENTS

TABLE OF CONTENTS (Continued)

Page

LIST OF FIGURES

LIST OF FIGURES (Continued)

LIST OF TABLES

LIST OF VARIABLES USED THROUGHOUT DOCUMENT

Variable:	Definition:
h	Height above DTM
t	Slice thickness
Δh	Half of slice thickness
h_i	Height of point i
z_i	Elevation of point i
z_{DTM}	Elevation on DTM at point i
r	Tree radius
r_{typ}	Typical tree radius
Δ	Grid (cell) size
M	Number of trees detected
N	Number of points detected in dataset
N_{min}	Number of points in dataset used to fit a circle to the tree
$\dot{x}$	Average x value
$\dot{y}$	Average y value
S	Summation of residuals
δ	Displacement
δx	Displacement in x direction
δy	Displacement in y direction
δxy	Total displacement
d	Tree diameter
s	Tree spacing

r_f	Scanner range filter distance
(X_c, Y_c)	Coordinates for the center of the tree in dataset coordinate system
(u_c, v_c)	Coordinates for the center of the tree in local coordinate system specific to each block of nine grid cells
Δr	Difference in radii between consecutive surveys

1 INTRODUCTION

This thesis describes a new technique to determine coastal erosion and movement along an actively moving coastal landslide. Specific research objectives are to:

- Develop an effective algorithm to monitor landslide movement using natural features such as tree trunk displacements
- Quantify the variability of displacement across the landslide
- Distinguish coastal advancement or retreat of the coastal bluff

This thesis follows the manuscript format.

Chapter 2 is a literature review providing a background of Light Detection and Ranging (LIDAR) from various platforms and Oregon Coastal landslides. Specifically, the Johnson Creek Landslide located approximately seven miles north of Newport and one mile south of Otter Rock is discussed. Research documents were obtained from peer-reviewed journals, technical reports, websites, and conference proceedings.

Chapter 3 presents a manuscript describing a new algorithm to automate landslide movement detection in a forested area using tree displacement. The purpose of this study was to determine the displacement of tree trunks within a coastal landslide using terrestrial laser scanning (TLS) to distinguish landslide

movement and erosion for a coastal landslide with a case study of Johnson Creek Landslide.

Chapter 4 provides overall conclusions of this thesis and discusses potential approaches for future research on monitoring landslide movement.

2 LITERATURE REVIEW

Coastlines continuously change due to erosion from dynamic environmental conditions. As polar ice caps melt, increasing the amount of water in the oceans, global sea level rises and water distribution around the world shifts resulting in continual changes in erosional patterns (Intergovernmental Panel on Climate Change, 2007). Many coastlines consist of unconsolidated sediments making them among the most easily erodible of all landforms (Priest & Allan, 2004). Furthermore, water is constantly circulating around the earth as tides cyclically pulls the oceans. As the water circulates, sediments are picked up from beaches and bluffs, causing erosion. Coastal erosion is determined by how much a beach or sea cliff retreats from the ocean due to waves, currents, wind, rainfall, or drainage removing sediments. However, when an active landslide located on the coastline is moving towards the ocean, the amount of erosion taking place is actually a result of the displacement of both the landslide movement and the retreat of the sea cliff. Hypothetically, if a bluff that is ten meters high and 100 meters long does not retreat from the ocean over one year the erosion results show no sediments lost, but if the bluff is part of an active landslide that advanced toward the ocean one meter, 1,000 cubic meters of sediments were actually transferred to the marine environment. These differences can be difficult to distinguish using conventional measurement and monitoring techniques.

This chapter will discuss several methods of laser scanning capable of documenting and measuring landscape change, contributing factors to Oregon coastal landslides and erosion, and previous work completed at Johnson Creek Landslide (JCL). Jaboyedoff et al. (2012) presents a comprehensive review of applications of light detection and ranging (LIDAR) for landslides concluding that four main applications: (1) detection and characterization of mass movement, (2) hazard assessment and susceptibility mapping, (3) modelling, and (4) monitoring. Within these applications airborne laser scanning showed valuable results at the region scale and terrestrial laser scanning effectively provides specific details.

2.1 LASER SCANNING OVERVIEW

LIDAR is an active optical remote sensing technology that measures the distance and angle to an object from a scanner using two primary techniques, time-of-flight measurement and phase measurement, to create complete 3D models with XYZ coordinates, termed point clouds. Scanners are a line of sight technology: once the complete laser pulse reflects from an object no points are detected behind the object causing occlusion. When only part of the laser pulse reflects back from a thin object, multiple returns can occur. Multiple returns means that when part of a laser pulse is returned, the rest of the pulse continues on until it reflects back to the scanner and multiple XYZ

coordinates are obtained from one laser pulse. To aid in identification of specific points, most scanners are capable of taking calibrated photographs to associate red, green, and blue (RGB) values to each point. Intensity or the strength of the return for each point is recorded, which aids in classification of the point. The intensity varies based on distance from the scanner and provides additional information about the material or composition of the point. Figure 2-1 shows how intensity is helpful in distinguishing objects of equal elevation such as the reflective striping of a road from the road itself (Vosselman & Maas, 2010).

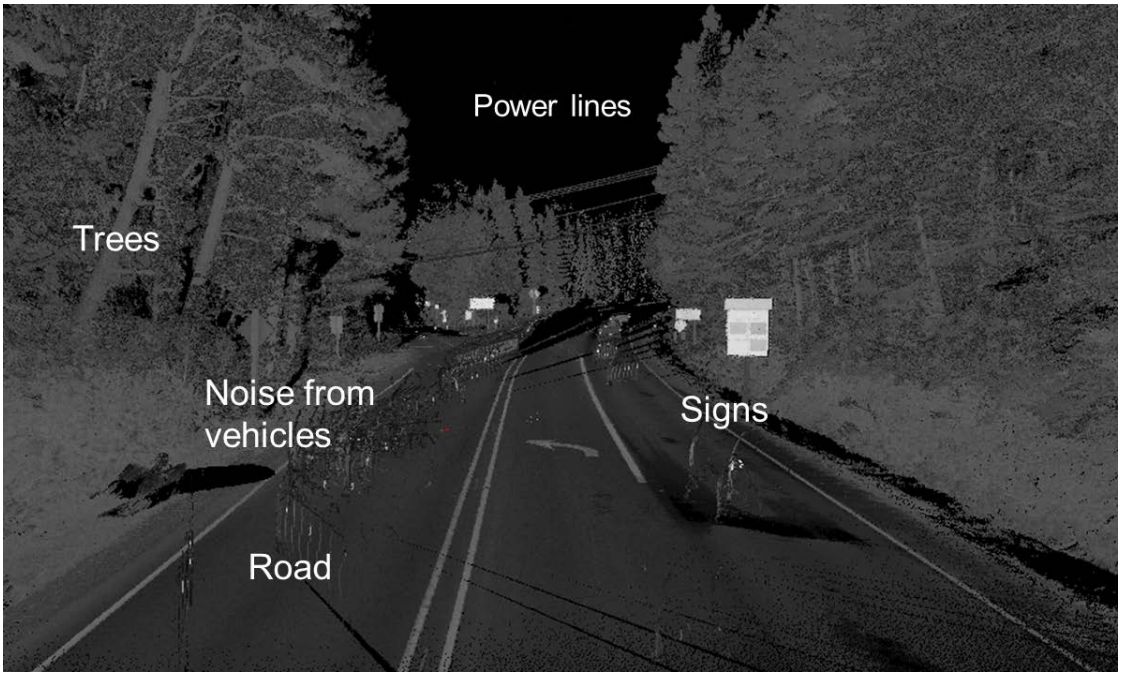

Figure 2-1 A 3D point cloud using intensity coloring to distinguish the reflective striping of a road from the road itself.

In both phase based scanners and time-of-flight scanners the position of each reflected object is relative to the scanner location known as a local coordinate system. Georeferencing data transfers points from a local coordinate system to a global coordinate system. As discussed by Wehr and Lohr (1999), phase measurements use a continuous wave (CW) laser to emit a constant sinusoidal signal to determine distance by the phase shift between the transmitted and received signal. Phase measurement systems record at a higher data rate and have a higher degree of accuracy (micro-meter level) compared to time-of-flight measurements. However, phase measurement systems are limited by their operational range to generally less than 80 meters. Therefore, the use of time-of-flight scanners, which have longer operational ranges, between 160 - 6000 meters, are more practical for most topographic mapping applications. Time-of-flight (TOF) scanners use the speed of light and two way travel time opposed to the phase shift between signals. The two way travel time starts when a laser pulse leaves the scanner and ends when the pulse returns to the scanner after reflecting off a target. Therefore, since light travels at a constant velocity for each medium, the XYZ position of each target is determined by emitting laser pulses and measuring the angle and two way travel time between the emitted and received pulse. The speed of light is determined by dividing the speed in a vacuum by the refractive index of the medium. Even though occlusion occurs with TOF

scanners, each pulse may have multiple returns or echoes. These returns aid in identifying objects, such as limbs on trees, and the final echo is usually returned from the ground. The number of echoes returned varies by scanner. The use of time-of-flight scanners is dominant in three main areas of topographic mapping: terrestrial laser scanning (TLS), airborne laser scanning (ALS) and mobile laser scanning (MLS).

2.1.1 Terrestrial Laser Scanning

Terrestrial laser scanners are preferably used for smaller regions, generally less than a few square kilometers. Current terrestrial scanners acquire data from tens of thousands to millions of points per second. Typically, longer range scanners use a lower pulse rate. The nominal precision (1 sigma) ranges from about 3 - 10 mm among various scanners on the market. However, results are difficult to compare between scanners because there is no standard method for testing the accuracy of scanners. TLS are usually setup on a tripod in a static position as shown in Figure 2-2 below. Multiple scan locations are required to observe all aspects of the same object.

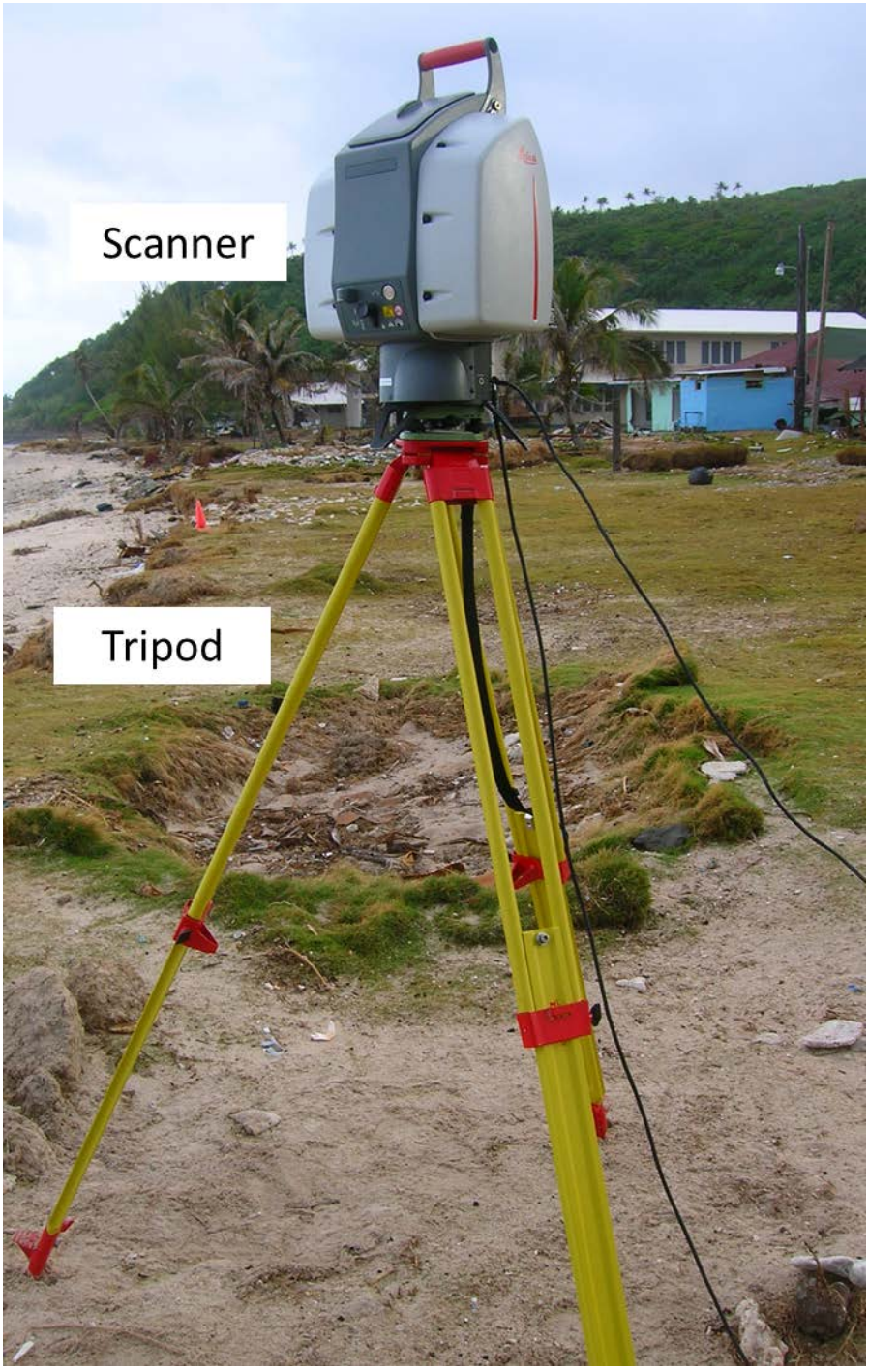

Figure 2-2 Typical Terrestrial Laser Scanner setup on a standard tripod

Laser scanning has been implemented for geological characterization and assessments of landslides. Collins and Sitar (2008) used TLS to show that bluff failures occurred from either wave action erosion or from precipitation induced groundwater and surface water discharge through the bluff face in weakly lithified sands. Dunning et al. (2010) integrates the use of TLS derived topographical and structural geological information for numerical modeling of a landslide in the Himalaya of eastern Bhutan. Collins and Stock (2012) discusses how both ALS and TLS can be used to conduct volumetric, structural, and deformation analysis of rock-fall areas.

2.1.2 Airborne Laser Scanning

Airborne laser scanning is commonly performed by using a low flying fixed wing aircraft. The scanner is fixed to the underbelly of an aircraft, which provides a near vertical look angle with a limited swath. Aerial laser scanning is referenced using onboard GPS units that typically record position twice per second and complimented by an inertial measurement unit (IMU) that has a sampling rate exceeding 100 Hz dependent on the unit type. In addition to fixed wing aircrafts, rotary wing has been used to conduct airborne laser scanning. Most helicopters that perform aerial laser scanning are capable of mounting the laser scanner in a traditional nadir look as well as an oblique configuration. Oblique helicopter laser scanning allows for an improved look

angle compared to fixed wing aerial scanning of steep cliffs. ALS provides precision usually ranging from 5 – 25 cm in operation.

Burns and Madin (2009) developed a protocol showing ALS beneficial to map landslides in Oregon compared to other remote sensing datasets, creating landslide hazard maps to help affected communities become more resilient.

Young et al. (2010) performed a comparison with TLS of sea cliff erosion and concluded that ALS has superior coverage that captures cliff-top and crest, which is useful for detecting large or deep seated landslides, but does not detect specific landslides or small scale change that can be detected by a TLS.

2.1.3 Mobile Laser Scanning

Mobile laser scanning materialized in the latter part of the past decade. Mobile scanners were designed with the same concept as airborne scanners, with the use of GPS and an IMU to provide continuous position and orientation information. They commonly have multiple laser scanners setup on one platform from various look angles to prevent occlusion. MLS typically use vehicles, but can also use trains or boats as a platform. Specifications for MLS accuracies (1-σ) range between 2 - 50 cm and collects measurements at rates of tens of thousands points per second to millions of points per second.

Several agencies have started using MLS in aspects such as asset inventory. For example, Lehtomaki et al. (2011) presents the application of using segmentation to extract poles and tree trunks from urban areas using MLS. Segmentation was used due to a lower point density than TLS and noise, which allows for only part of the cylindrical targets to appear. Although some trees were detected that were uniformly spaced along the road the tree canopies were problematic.

2.1.4 Scanning Comparison

Laser scanning is a rapidly emerging survey technique. For the past decade scanning technology has continuously evolved and improved. It is important to look at all three methods of scanning and various scanners before deciding the best approach for any project. Lemmens (2010), GIM International (2011) and Puente et al. (2011) review several different laser scanners and their specifications, which are summarized in Table 2-1. Table 2-2 summarizes some of the advantages and disadvantages of the various scanning methods.

Table 2-1 Specification comparison of scanning methods (Data obtained from (Lemmens, 2010), (GIM International, 2011) and (Puente et al., 2011))

	TLS	ALS	MLS
Typical scan range (m)	1 – 100	1000	1 – 100
Data Acquisition Rate (kHz)	5 – 300	30 – 500	40 – 1,000
Accuracy – 1 std deviation (mm)	3 – 10	20 – 70	2 – 50
Beam Divergence (mrad)	0.12 – 0.30	0.22 – 2.7	0.19 - 0.3
Spot Size (mm) @ 500m	70 - 150	102 - 1250	100 - 200
Point Density (# points per sq. meter)	Highly variable, > 10000 close to scanner	8 – 175	Highly variable, > 5000 close to vehicle path

Table 2-2 Advantage and disadvantage of measurement technique for sea cliff erosion of landslide

Technique	Advantage	Disadvantage
1. Terrestrial Laser Scanning	• Best accuracy • Highest resolution • Temporal coverage	• Limited spatial coverage • Requires georeferencing
2a. Fixed Wing Aerial Laser Scanning	• Spatial coverage • Continuous dataset • Uniform sampling	• Look angle for vertical objects • Complex planning
2b. Helicopter Aerial Laser Scanning	• Improved look angle from 2a (Oblique) • Capable of following complex corridors • Greater point density than 2a	• Complex planning • Slower than 2a
3. Mobile Laser Scanning	• Better accuracy than 2a and 2b • Best data acquisition rate • Continuous dataset • Better uniform sampling than 1	• Restricted to roads, trails, or railways • Range • Data storage

An advantage of TLS for sea cliff scanning is that it is very accurate and has a preferred look angle because it is more orthogonal to vertical cliffs compared to ALS. Young et al. (2010) determined that a preferred look angle, when target surfaces are perpendicular to the laser, minimizes grazing angle errors and the best results are achieved, TLS can capture the trunks of trees in highly vegetated areas. The temporal coverage of an area or object can range from hourly, weekly, or annually depending on the requirements or limitations of the person performing the scans. One limitation of TLS is that data from each setup location must be georeferenced and are not a continuous dataset. Due to the need for multiple setups, optimally every 50 meters, it is difficult to get large spatial coverage from TLS (Olsen et al., 2009).

Airborne laser scanning has the capability of covering a very large area and maintains continuous data as one large dataset (Buckley et al., 2008). Despite the advantages of ALS, there are substantially more logistical concerns and cost associated with planning, flying and processing flight missions for ALS.

MLS provides a much denser point cloud than ALS because of the data acquisition rate. However, MLS are limited by their range, typically less than 200 m and maximum range of 500 m in optimal conditions, and the amount of

data storage space required because of the point density (Puente et al., 2011). Data quality degrades significantly with increased distance.

2.2 NORTHERN OREGON COAST

The northern Oregon coast extends south from the mouth of the Columbia River to Florence (Figure 2-3). North and Byrne (1965) determined that land sliding is active along 130 of the 240 kilometers of coastline. Further, adding to the threat of additional landslides, the Cascadia Subduction Zone extends under the coast range where the North American tectonic plate is overriding the Juan de Fuca plate 60 - 120 km west of the coast (Mitchell et al., 1994).

Figure 2-3 Map showing extents of northern Oregon coast. Base map photographs provided by ESRI.

2.2.1 Geologic Setting

The most common lithological units for the northern Oregon Coast are: sedimentary rock (53 km), igneous rock (60 km) and beach, dune sands (129 km) (North & Byrne, 1965). The most common exposed rocks are (1) tertiary marine sediments varying in age from Eocene to Miocene Epochs, 58 to 22 million years old respectively, and (2) igneous rocks of Eocene and Miocene age, which are the most resistant to erosion (North & Byrne, 1965). Sediments of Pleistocene age, 2 million years old, make up the terrace caps atop of the Tertiary rocks.

Within Lincoln County, Oregon, there are several translational landslides moving through Tertiary sedimentary rocks with coastal bluffs 20 - 60 meters high (Priest et al., 2011). The tertiary period ranges from 6 to 63 million years old. Priest and Allan (2004) describe these landslides from the Miocene age as thick to thin-bedded, very fine to medium grained, micaceous and carbonaceous arkosic sandstone and massive silty sandstone and are common with single block failures exceeding 100 meters in width. This formation dips 10 – 30 degrees west and has poorly defined bedding consisting of mostly clayey, sandy siltstone (Schulz et al., 2012).

2.2.2 Slope Failure

Landslides are a persistent problem along the Oregon coast that results from downward sliding of an earth mass. Komar (1998) stated that the common ingredient of landslides is gravity, which causes the downward and outward movement of mass. Gravity is only part of the problem for slope failures. Fernandez Merodo et al. (2004) states that slope failures are caused from (1) changes in the effective stresses (e.g. rainfall or loading), (2) variation of material properties, or (3) changes in geometry. Therefore, landslides happen when driving forces (gravity or loading of the slope) exceed resisting forces (shear strength) and material with higher shear strength can form steeper slopes before failing.

2.2.3 Coastal Erosion

The Oregon coast experiences both beach erosion and sea cliff erosion, which are problems for land development (Komar, 1998). The ocean is one of the main contributing causes of erosion along the coast, but within the ocean itself there are many contributing factors such as: wave action, cell circulation with rip currents, tidal variations, storm surge and sea level change. These ocean factors cause erosion to beaches, dunes, and sea cliffs. The amount of coastal erosion varies depending on the physical volume of beach sediments, the composition and grain size, and the presence of drift logs.

Seacliff erosion can be more severe and varies not only because of factors associated with the cliff such as: composition, layering, inclination of rock layers, and height and slope of cliff face, but also because of external factors such as: rain wash on the face, ground water flow and pore pressure, vegetation, burrowing by rodents, and the actions of people. When a sea cliff experiences significant erosion complete failure can occur and damage infrastructure (e.g., homes, roads, and parks) atop of the cliff.

Seacliff erosion is comprised of both marine and subaerial mechanisms. Young et al. (2009) states the marine processes as wave-driven, directly acting only at the cliff base. Erosion on the base of the cliff develops sea caves or erodes the toe of the sea cliff causing destabilization. Subaerial mechanisms, such as groundwater processes and slope wash, act over the entire cliff face and erode the cliff from the top and works toward the ground.

Temporal coverage of sea cliffs using LIDAR has proven to be an effective way to monitor sea cliff erosion and volumetric change. Rosser et al. (2005) monitored the erosion of near vertical hard rock sea cliffs using TLS to quantify cliff failures. Young et al. (2009) compared repeat ALS datasets over four years to assess the roles of wave attack and rainfall on erosion of sea cliffs, concluding that the combined effects accelerate erosion; upon reactivation of one landslide it experienced net erosion rates exceeding 20

times that of regional averages. Young et al. (2010) compared ALS to TLS for volumetric change concluding that deposition volumes were similar, but ALS detected significantly less erosion (31%). Due to the larger footprint of ALS many small changes go undetected reducing the amount of erosion determined.

2.3 JOHNSON CREEK LANDSLIDE PREVIOUS WORK

One of the most widely researched landslides along the Oregon Coast is located at where the Johnson Creek meets the Pacific Ocean. The Johnson Creek landslide is located about one mile south of Otter Rock and seven miles north of Newport along Highway 101 (Figure 2-4), the primary roadway connecting Oregon Coastal communities. The landslide has caused multiple roadway problems along the highway, and as it continues to erode, it threatens the entire coastal region, which relies on this route as their main connection. The damage the landslide has done required a complete realignment of the Old Coastal Highway and requires continual road repairs from movement. Schulz and Ellis (2007) report that the JCL is a translational landslide, one with little rotation, displacing through a coastal bluff and is primarily bedrock. It is nearly 360m wide, 200m long, with its toe exposed as a sea cliff along the west side. The landslide was first visible on 1939 aerial photographs. Although Oregon Department of Transportation (ODOT)

installed six inclinometers during 1970, it was not until 2002 that detailed investigation of the landslide began using subsurface exploration, numerical modeling and LIDAR.

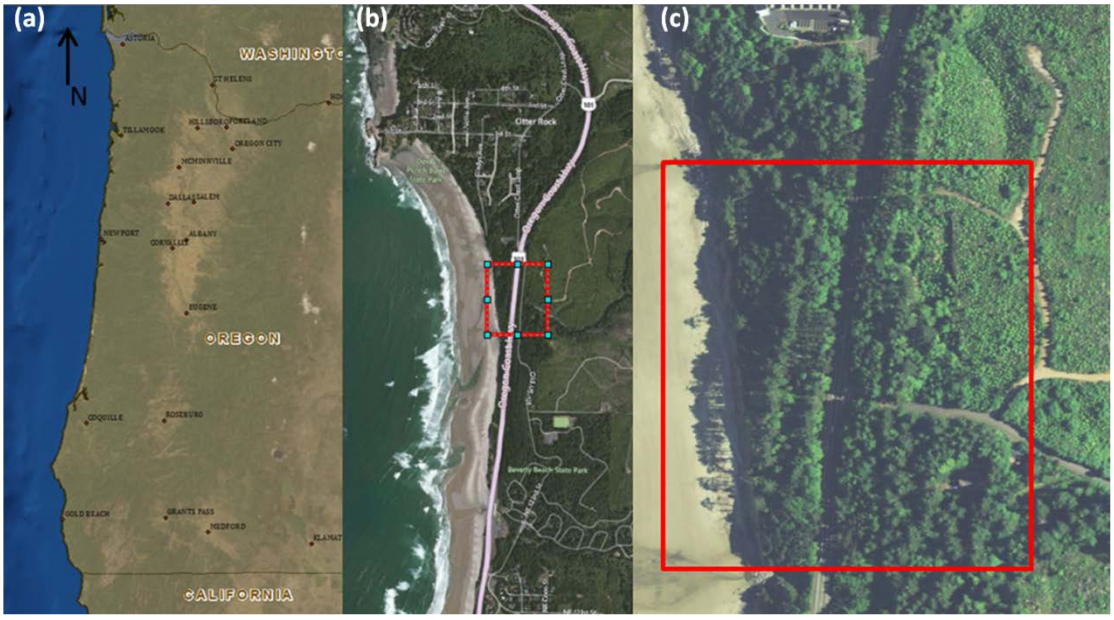

Figure 2-4 Location map, reference to Oregon and Otter Rock: (a) is a map of Western Oregon, (b) shows HWY 101 from Newport to Otter Rock, and (c) is a plan view of JCL. Base map photographs provided by ESRI.

2.3.1 Subsurface Exploration and Monitoring

Subsurface exploration of the JCL began in late 2002, as a combined effort between ODOT and Oregon Department of Geology and Mineral Industries (DOGAMI), with three pairs of boreholes constructed along a longitudinal section (Schulz & Ellis, 2007). One of the boreholes in the pair had piezometers installed to measure groundwater pressure and temperature.

Inclinometer casings were installed in the other boreholes to measure landslide movement. Eventually landslide movement was so excessive that it prevented the inclinometer survey; therefore, manual extensometers consisting of wire rope were installed in the three inclinometer casings to obtain measurements of landslide movement. To measure rainfall, a tipping bucket rain-gauge was installed. The piezometers and rain-gauge collected readings hourly by a battery powered data logger. The extensometer required manual readings at irregular intervals. Landslide Technology (2004) provides complete details of the 2002 study and instrumentation used. This report concluded that groundwater pressure was the primary cause of movement.

In November 2004, the United States Geological Survey (USGS) Landslide Hazards Program in cooperation with DOGAMI began upgrades to the instrumentation and monitoring of the JCL. Two automatic data loggers were installed, one on each side of Highway 101, allowing simultaneous readings of precipitation, groundwater pressure and landslide movement of the JCL (Schulz & Ellis, 2007). The automatic data loggers were initially collected by routine site visits until January 2006, when cellular modems were added to the data loggers for remote collection of data. Schulz and Ellis (2007) document complete details of the changes made to the monitoring network during 2006 at JCL. These changes include the installation of fourteen more piezometers in four new boreholes. Two of the boreholes were created within

a few meters of the 2002 boreholes, which contain vertical array of six piezometers each. The remaining two piezometers are located inside a slotted well casing near the bottom of the other two boreholes. Four shallow soil water-content sensors, an air temperature sensor and cable-extension transducers to the manual extensometer were also installed. The data collection rate was increased from every hour to every fifteen minutes. Results revealed that the middle section appeared to control the movement of the entire slide and small movements appeared to move the entire slide equally and simultaneously, but larger movements affect the middle of the slide greatest followed by the west and least in the east (Priest et al., 2008).

2.3.2 Numerical Modeling

Priest et al. (2008) presents slope stability analyses completed by two independent groups using standard of practice limit equilibrium methods to evaluate the influence of groundwater conditions, geotechnical parameters and toe erosion on the landslide movement. The modeling was performed on multiple cross sections of the slide using conventional 2-D slope stability procedures to determine the 3-D movement of the entire landslide. Both studies used the same method and computer program XSTABL to back-calculate the required strength or residual friction angle to develop failure conditions (Interactive Software Designs, 2011). A higher value obtained for the residual friction angle is interpreted as less stable.

The first analysis was conducted by Landslide Technology using data available in 2002 and the spring of 2003 along a cross section intersecting the drilling sites of the six boreholes constructed in 2002 (Priest et al., 2008). The data used for analysis was: 1) borehole data (inclinometer and piezometer readings), 2) depth of sliding and groundwater data from instrumentation, 3) geologic reconnaissance of the site and 4) topographic map. Landslide Technology's analysis determined a residual friction angle of 6.5 degrees to start movement of the landslide and the largest reduction in the factor of safety was caused by increased groundwater pressure from a severe storm. Erosion of the cliff face caused a slightly lower reduction in the factor of safety. The seasonal movement of sediments had a minimal impact on the factor of safety.

The second analysis was conducted by Samuel Christie and Dr. Stephen Dickenson of Oregon State University. Priest et al. (2008) presents their objectives as verifying the previous results of Landslide Technology and to expand the analysis from one to three cross sections for the influence of groundwater conditions and geotechnical parameters. To verify the results of Landslide Technology one cross section was along the boreholes similar to the cross section tested by Landslide Technology. To expand the analysis an additional cross section to the north of the 2002 boreholes with another one south of the boreholes were examined. The residual friction angle for the similar cross section was 5.9 degrees. Higher maximum residual friction

angles were determined for the northern and southern cross sections, 5.7 to 8.3 degrees and 9 to 11 degrees respectively. The highest number in the southern section indicate it is the least stable, which agrees with increased movement for this portion of the landslide. Their analysis also determined that water filled cracks going deeper than ~8 m can destabilize the base of the cliff (toe) and failure to the toe would cause instability of the entire landslide.

Schulz et al. (2012) used field mapping, subsurface exploration, in situ monitoring of rockslide movement and hydrologic conditions of three Oregon coastal landslides (Johnson Creek, Camel Knoll, and Devils Punchbowl), determining seismic loads would trigger formation of rockslides. Also, likely intense rainfall events account for annual movement of these landslides. Gravitational instability indicated short failures located along the bluff face. This study also concluded that JCL was likely triggered by the last great Cascadia subduction zone earthquake in 1700.

2.3.3 Laser Scanning

Laser scanning of JCL was originally not part of ODOT's and DOGAMI's original plan to monitor landslide movement, but proved to be necessary in documenting the erosion of the bluff face including the toe of the slope. Priest et al. (2008) identified that the use of erosion monitoring pins were initially expected to monitor total toe erosion, but most of the pins were lost during the

first season, preventing their use. In May 2004, ODOT and DOGAMI conducted an initial test of laser scanning at three isolated locations each one about 50 meters wide across the bluff face, similar to the example point cloud in Figure 2-5 below. Scans of the entire bluff face followed in October 2006 and April 2007. Limited processing capability prevented them from capturing the total landslide movement along the bluff. Results revealed that the profile change between 2004 and 2007 is less in the north and increases to the south. These laser scans also indicated that erosion is much greater at lower elevations than the higher parts of the bluff. They also reveal that erosion is greatest in the south and least in the north. The 2007 laser scan placed the entire bluff west of the 2006 scan indicating the landslide movement exceeded the rate of erosion.

Figure 2-5 Colored point cloud from digital images of a 50 meter section Johnson Creek Landslide

The Oregon State University Civil Engineering Geomatics Lab completed additional surveys of JCL, as shown in the table below (Table 2-3). These

surveys exceeded the extents of the entire landslide bluff in an effort to distinguish landslide movement from active erosion. An example point cloud is presented in Figure 2-6 below. Olsen et al. (2012a) used these scans in conjunction with the previous scans by ODOT to estimate landslide movement by manual extraction and comparison of features (houses, trees and stairwells) on top of the landslide between the 2007 and 2011 surveys. These surveys conducted prior to 2012 consisted of only scans along the bluff face. This study concluded that areas of high erosion also experience significant landslide movement such as the southern portion of the landslide. Areas such as the north that experience little erosion have considerably less landslide movement.

Table 2-3: Terrestrial laser scan surveys completed of JCL bluff face by OSU. (Table modified from (Olsen et al., 2012b)).

Date	Surveyor	# scans	#points ($x10^6$)	Alignment Error (RMSE, cm)
12/2010	OSU	8*	120	3
06/2011	OSU	8*	115	2
08/2011	OSU	7*	115	3
04/2012	OSU	25**	703	4
11/2012	OSU	26**	699	4

* = the scans used for this analysis were extracted from a much larger survey covering a longer section of the coast.

** = the scans used for this analysis include scans of the bluff face and the top of the landslide area. Other surveys only include the bluff face.

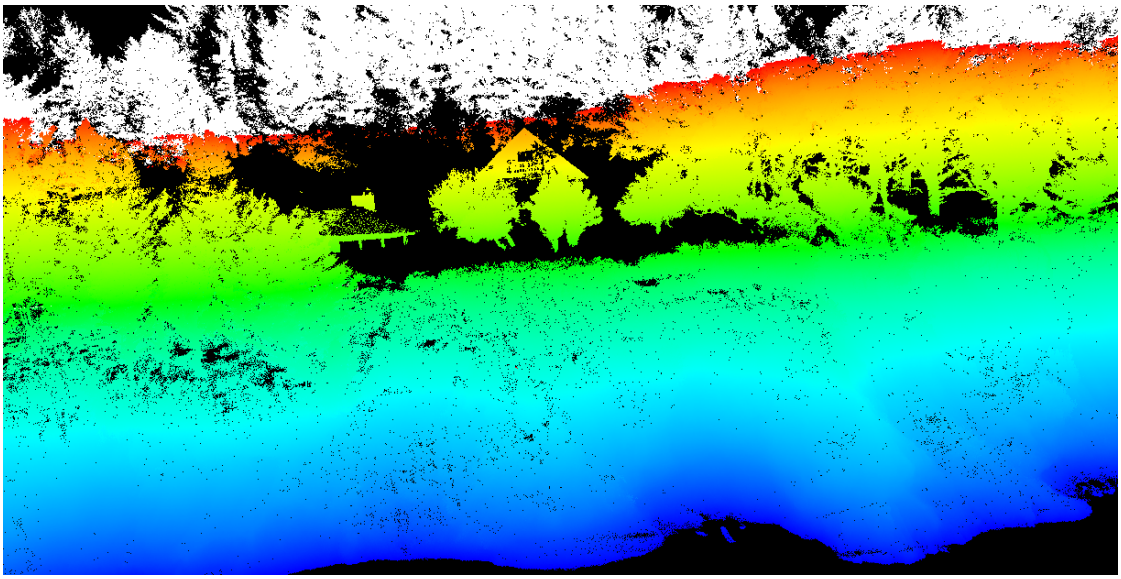

Figure 2-6 Point cloud of JCL showing a 60 m section of bluff face with trees and houses on top of the bluff, colored by elevation.

2.4 CONCLUSIONS

JCL is a very active landslide with an eroding bluff that captures the attention of researchers due to its aggressive movement rates. Priest et al. (2008) and Olsen et al. (2012a) have shown that the landslide moves fastest in the southern section and slows northward. Priest et al. (2006), Schulz and Ellis (2007) and Priest et al. (2008) determined that the landslide does not move at the same rate moving east from the bluff. These studies focus on a few test areas within the JCL that do not connect or extend past the landslide block. Most of the subsurface exploration was done in a nearly straight longitudinal section limiting the scope of results. This study will have an

improved characterization of landslide movement that distinguish landslide movement from erosion to calculate an improved sediment loss rate. It will also have an improved distribution across the site and provides a systematic approach for future monitoring.

3 MANUSCRIPT CHAPTER

Automated quantification of distributed landslide movement using circular tree trunks extracted from terrestrial laser scan data

Jeremy C. Conner[1], Michael J. Olsen[2]

1. Major, United States Army, School of Civil and Construction Engineering, Oregon State University, 220 Owen Hall, Corvallis, OR, 97331, jeremy.conner1@us.army.mil
2. Assistant Professor, School of Civil and Construction Engineering, Oregon State University, 220 Owen Hall, Corvallis, OR, 97331, michael.olsen@oregonstate.edu

3.1 ABSTRACT

This manuscript presents a novel algorithm to automatically detect landslide movement in a forested area using displacements of tree trunks distributed across the landslide surveyed repeatedly using terrestrial laser scanning (TLS). Common landslide monitoring techniques include: inclinometers, global position system (GPS), and interferometric synthetic aperture radar (InSAR). While these techniques provide valuable data for monitoring landslides, they can be difficult to apply with adequate spatial or temporal resolution needed to understand complex landslides, specifically in forested environments. Comparison of the center coordinates (determined via least-squares fit of the TLS data) of a cross section of the tree trunk between consecutive surveys enable quantification of landslide movement rates, which can be used to analyze patterns of landslide displacement. The capabilities of this new methodology were tested through a case-study analyzing the Johnson Creek Landslide, a complex, quick moving coastal landslide, which has proven difficult to monitor using other techniques. A parametric analysis of fitting thresholds was also conducted to determine the reliability of tree trunk displacements calculated and the number of features that were extracted. The optimal parameters in selecting trees for movement analysis were found to be less than 1.5 cm for the RMS residuals of the circle fit and less than 1.0 cm for the difference in the calculated tree radii between epochs.

3.2 INTRODUCTION

Landslides are persistent natural hazards that result from downward sliding of an earth mass. Landslides can be triggered by a variety of factors such as precipitation, groundwater fluctuations, seismic activity, erosion, and human activities which destabilize the slope through geometric or loading changes (Fernandez Merodo et al., 2004). They have both direct and indirect effects on people and the environment. Large landslides can destroy or damage everything in their path when a failure occurs (i.e. people, roads, houses). Further, the immediate impact of a landslide is often overshadowed by the aftermath. Landslides often damage or block roadways that are necessary to link remote population centers, causing hardship for everyone affected.

3.2.1 Landslide Monitoring

Landslide movement is often determined be a wide variety of monitoring techniques, including inclinometers, GPS, InSAR, and LIDAR. These techniques each have positive and negative attributions for landslide monitoring dependent on landslide characteristics. This section will discuss these techniques, with the exception of LIDAR, which will be addressed in more detail in the following section.

Wieczorek and Snyder (2009) describe using inclinometers to monitor movement at discrete locations on a landslide by placing a hollow metal tube inside a drilled hole and periodically monitoring the variation of the original inclination of the tube. Although inclinometers provide subsurface detail of landslides, which other techniques do not capture, they have poor spatial resolution. They can also break when a landslide moves too quickly.

Permanently mounted GPS units have been used to monitor surficial landslide movement by analyzing positional changes of the GPS units compared to stable units in a GPS network. Wang (2011) showed landslide movement could be determined by GPS within 2 mm horizontally and 6 mm vertically with four hour observations and an open view of the sky. However, the cost of permanently mounting the survey-grade GPS units necessary for this detection is too high to mount more than a few receivers on a single slide, limiting spatial resolution and the number of landslides that can be monitored. Often this is only sued for landslides near high population areas.

Interferometric Synthetic Aperture Radar (InSAR) determines displacement from the phase change between radar images. Rosen et al. (2000) describes how vegetation canopies affect InSAR imaging by reporting a height of somewhere between the ground and the top of the canopy and reduces correlation between images because of volumetric scattering.

Hence, it can be very difficult to apply for landslide monitoring in heavily forested environments. InSAR provides increased spatial coverage, but is limited in temporal coverage by repeat passes.

3.2.2 LIDAR Background

Light Detection and Ranging (LIDAR) is an active optical remote sensing technology that measures the distances and angles to objects from a scanner to create complete 3D models of XYZ coordinates, termed point clouds. A laser pulse is emitted from the scanner, reflects off a target, and returns to the scanner, providing the two way travel time used to determine the distance from the scanner for each target. Scanners are a line of sight technology: if the complete laser pulse reflects from an object, no points are detected behind the object, creating an occlusion (shadow). When only part of the laser pulse reflects back from a small object, the remaining light continues and multiple XYZ coordinates (returns) can be obtained from one laser pulse (Renslow, 2012). Multiple returns enable improved penetration of vegetation canopy compared to many other techniques.

LIDAR has proven to be an effective tool for landslide analysis ranging from detection and characterization of mass movement and monitoring at the regional scale with airborne laser scanning to terrestrial laser scanning (TLS) providing site specific details at improved resolutions (cm level) (Jaboyedoff et

al., 2012). TLS has been successfully implemented for geological characterization and assessment of landslides (Collins & Sittar 2008; Dunning et al. 2010; Collins & Stock, 2012).

Laser scanners have also proven to be an effective way to monitor coastal erosion and cliff collapses (Rosser et al. 2005; Olsen et al. 2009; Young et al. 2009). Young et al. (2010) performed a comparison between TLS and airborne laser scanning (ALS) for sea cliff erosion analysis and concluded that ALS has superior coverage capturing the cliff-top and crest, which is useful for detecting large or deep seated landslides but may not detect surficial landslides, erosion hotspots, or detailed change that can be picked up by a TLS. Monitoring areas of increased erosion and detailed change is necessary to understand the landslides occurring along the Oregon coast.

Several agencies have started using MLS in aspects such as asset inventory. For example, Lehtomaki et al. (2011) presents the application of using segmentation to extract poles and tree trunks from urban areas using MLS. Segmentation was used due to a lower point density than TLS and noise, which allows for only part of the cylindrical targets to appear. Although some trees were detected that were uniformly spaced along the road, the tree canopies were problematic. Hence, this approach is not suited for a heavy forest environment.

3.2.3 Study Area

The northern Oregon coastline extends south from the mouth of the Columbia River to Florence. Landslides are a persistent problem along the Oregon coast due to weak soils and high concentration of erosional processes, resulting in slope failures and coastal erosion. Erosion on the toe (base) of the sea cliff causes destabilization and can result in the formation of notches or sea caves. North and Byrne (1965) determined that land sliding is active along 130 of the 240 kilometers of coastline. Further, additional landslides can be triggered by seismic sources, such as the Cascadia Subduction Zone, which extends under the coast range where the North American tectonic plate is overriding the Juan de Fuca plate 60 - 120 km west of the coast (Mitchell et al., 1994). Within Lincoln County, Oregon there are several translational landslides moving through Tertiary (6 to 63 million years old) sedimentary rocks with coastal bluffs 20 - 60 meters high (Priest et al., 2011). Priest and Allan (2004) describe these landslides from the Miocene age as thick to thin-bedded, very fine to medium grained, micaceous and carbonaceous arkosic sandstone and massive silty sandstone and are common with single block failures exceeding 100 meters in width.

One of the most widely researched landslides along the Oregon coast is the Johnson Creek Landslide (JCL), located about one mile south of Otter Rock and seven miles north of Newport along Highway 101. JCL is a

translational landslide displacing through a coastal bluff and is approximately 360 meters wide, 200 meters long (Schulz & Ellis, 2007). Prior subsurface exploration of JCL has characterized and monitored the landslide movement (Landslide Technology 2004; Schulz & Ellis 2007; Priest et al. 2008). However, these efforts have been met with difficulty. Erosion pins were initially intended to monitor erosion, but too many pins were lost over the first winter season, preventing accurate determination of the total amount of erosion. Inclinometer casings were installed to measure landslide movement, but movement was so excessive that it prevented the inclinometer survey; therefore, manual extensometers of wire rope were installed to obtain measurements of movement. Landslide Technology (2004) and Priest et al. (2008) performed slope stability analyses to evaluate the influence of groundwater conditions, geotechnical parameters and toe erosion on the amount of landslide movement. The slope stability analyses determined the landslide is least stable in the southern portion of the landslide and increases in stability moving northward. Priest et al. (2008) and Olsen et al. (2012a) used TLS to model the erosion of the bluff face as well as landslide movement. Olsen et al. (2012a) estimate landslide movement by manual extraction and comparison of features (houses, trees and stairwells) along the crest of the coastal bluff face of the landslide, concluding that areas of increased landslide movement also experience more erosion. Hence, for

improved understanding and representation of the landslide movement, displacement needs to be monitored throughout the entire landslide area.

3.3 PURPOSE

The aim of this research is to develop an automated algorithm that determines landslide movement along an eroding coast in a forested area using dense, time-series data acquired using terrestrial laser scanning. Specifically, key objectives were to:

- Develop a consistent, systematic, monitoring technique using existing (natural), durable features since artificial instrumentation is often destroyed from landslide movement.
- Map displacement across the slide so that one can identify distinct landslide blocks and understand the complexities of non-uniform landslide movement.
- Distinguish between erosion and landslide movement components of change observed between repeat surveys.
- Evaluate the sensitivity of methodology to input parameters.

3.4 METHODOLOGY

To demonstrate the feasibility of the proposed methodology, the JCL, a highly active landslide, was selected as a test site. Trees are rigid natural

features that can withstand a significant amount of movement. Cross sections of tree trunks are also nearly circular in shape, enabling detection and extraction from a point cloud. Tracking the changes in the center coordinates of the circle over time provides a displacement vector. Multiple trees can then be detected across the site to map the entire landslide and examine variability in movement. An overview workflow for extracting displacements is outlined in Figure 3-1.

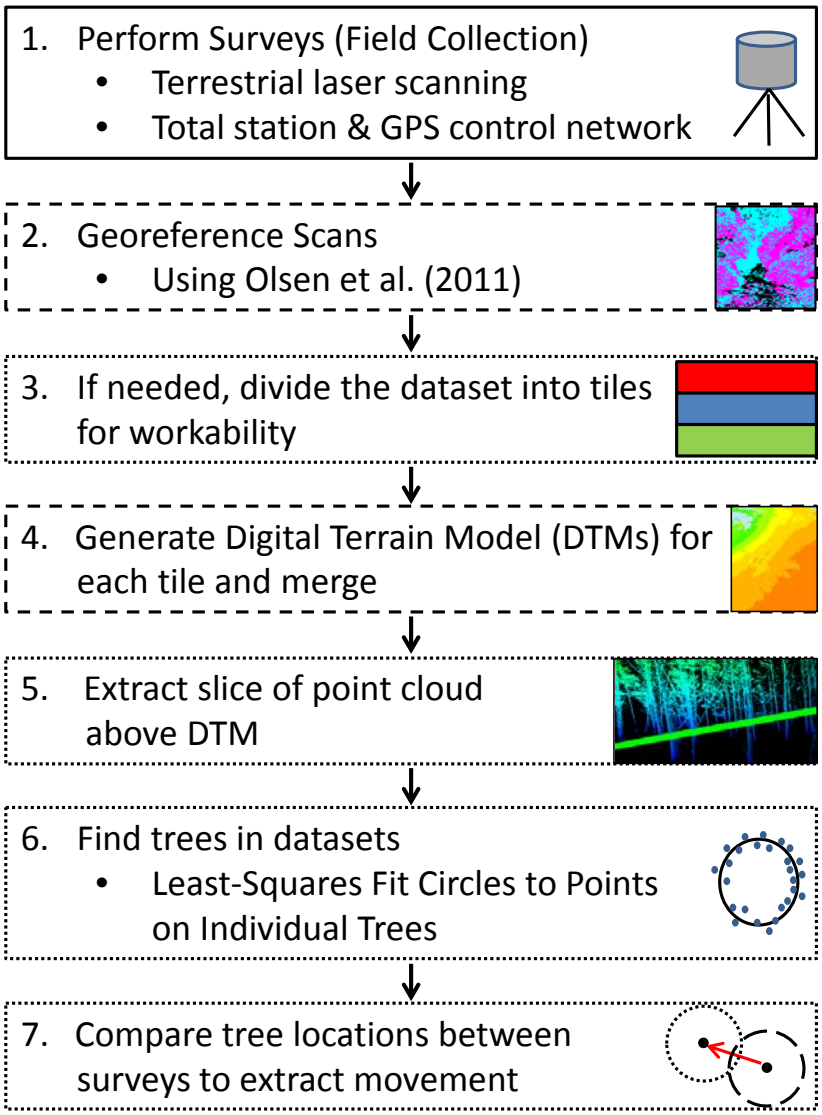

Figure 3-1 Workflow diagram for tree movement detection. Steps done automatically are shown with small dashes and semi-automatic steps are shown with large dashes.

3.4.1 Field Collection

Figure 3-2 shows the locations from which scans were obtained and methods used to obtain the coordinates for each survey. Control points were

setup using the Oregon Real-time GPS Network (ORGN), providing RTK GPS. For the RTK-GPS determined positions, three, one-minute readings per setup were collected, checked for consistency, and averaged. Scans conducted on the beach were completed with the GPS mounted on top of the scanner. On top of the sea cliff, vegetation and tree cover prevented GPS acquisition from all scan positions, requiring the use of a total station to tie into the control points. A Reigl VZ-400 scanner (nominal measurement accuracy of 5mm, 1 standard deviation, σ) was used for all scans; a five minute 360 degree scan with angular resolution of 0.03 degrees was collected from each scan position. Each scan collected an average of 27.5 million points per scan resulting in approximately 700 million points per survey.

Total station, a total positioning system that collect distances and angles, measurements were used to establish coordinates for scan origin markers placed across the site on top of the bluff. A Leica TPS 1200+ series total station was set up at two locations to determine coordinates of each of the 15 scan positions (reference points) on top of the sea cliff. The total station data collected was initially stored in a local coordinate system. The instrument height was measured and recorded three independent times varying by less than 0.1 cm, the average of the three readings was used as instrument height. The scanner was setup on a tripod over each reference point. The instrument height was measured and recorded three independent times varying by less

than 0.1 cm with the average recorded as the instrument height. GPS control coordinates were obtained from three locations with relatively clear views of the sky near the boundary of the landslide area. These three positions were also used as scan positions, as well as to constrain the overall network, as shown in Figure 3-2.

Geomorphological data were acquired along the beach to monitor erosion magnitudes and patterns on the bluff face. The scanner was mounted to a wagon to speed transport between scan positions as shown in Figure 3-3. The scans were conducted about 40 meters from the cliff and spaced 50 meters from one another. Olsen et al. (2009) describes these as the optimal zone for TLS of a dynamic coastal setting similar to JCL area.

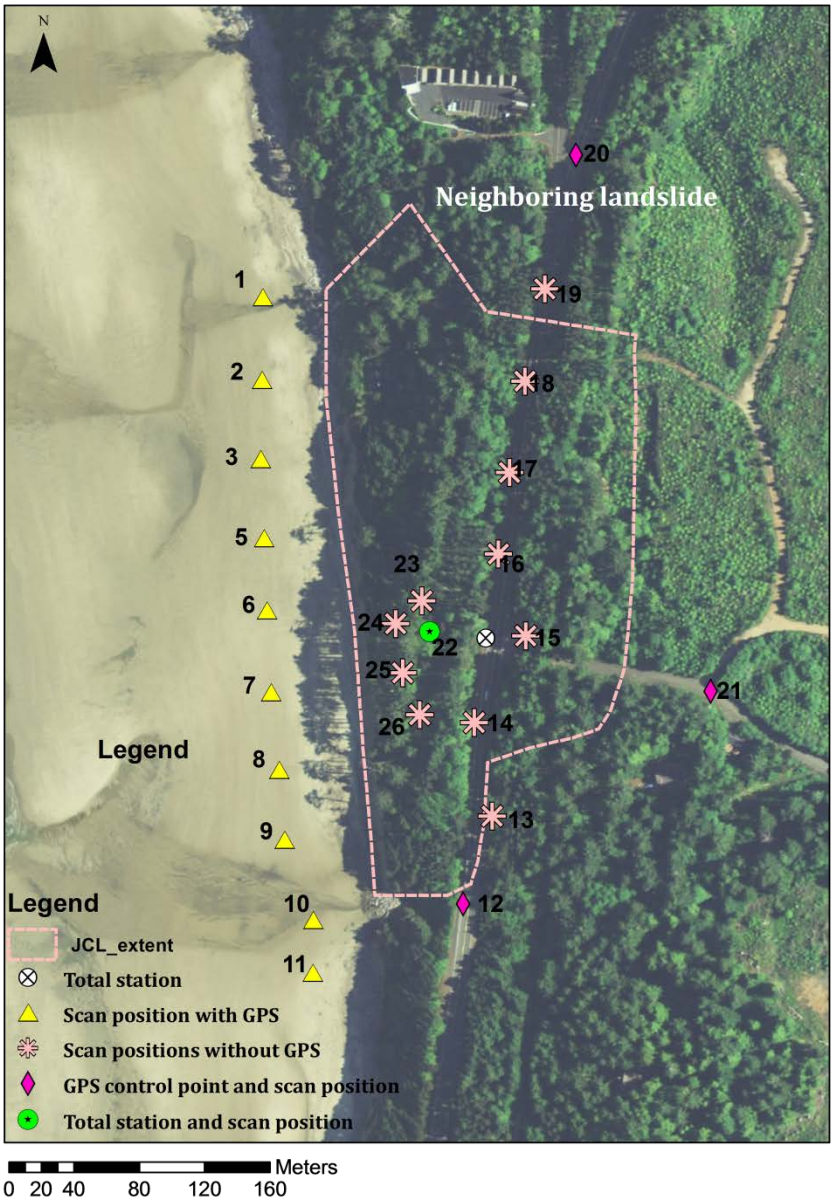

Figure 3-2 Test site layout of GPS, total station, and scanner origins. Base map photographs provided by ESRI.

Figure 3-3 Stop and Go laser scanner setup in modified configuration on a wagon.

3.4.2 Georeference Scans

In order to compare changes between surveys the data requires georeferencing into a common coordinate system. Figure 3-4 outlines the process for georeferencing the scan data collected following the procedure outlined in Olsen et al. (2009; 2011a). First, the three RTK GPS control points located on top of the landslide area were used to transform the total

station points into a global coordinate system. The GPS data for the April 2012 survey, varied by less than 1.5 cm for horizontal observations and vertical observations varied up to 5 cm. For the November 2012 survey, horizontal observations varied by less than 2 cm and vertical observations varied up to 5 cm. For both surveys, the observations from each control point were averaged for the final GPS location. The total station network was adjusted to the GPS points through a least-squares fit. For the April 2012 survey, horizontal residuals were less than 0.6 cm and vertical residuals were less than 5 cm. For the November 2012 survey, residuals were less than 2.5 cm (horizontal) and 5 cm (vertical). The adjusted points are the scan locations at ground level. In order to offset the scanner height, the measured instrument height is added to the adjusted points, resulting in coordinates for the scanner origins. PointReg, an automated program, inputs the scanner origin coordinates (X, Y, and Z) obtained using the previously described techniques, the roll and pitch from the inclination sensors of the scanner for leveling information and an initial yaw estimate (obtained by manually rotating the scans about the Z-axis to within a few degrees) to geo-reference all the scans (Olsen et al., 2011a). The algorithm performs a least-squares adjustment to determine the optimal yaw angles of all scans.

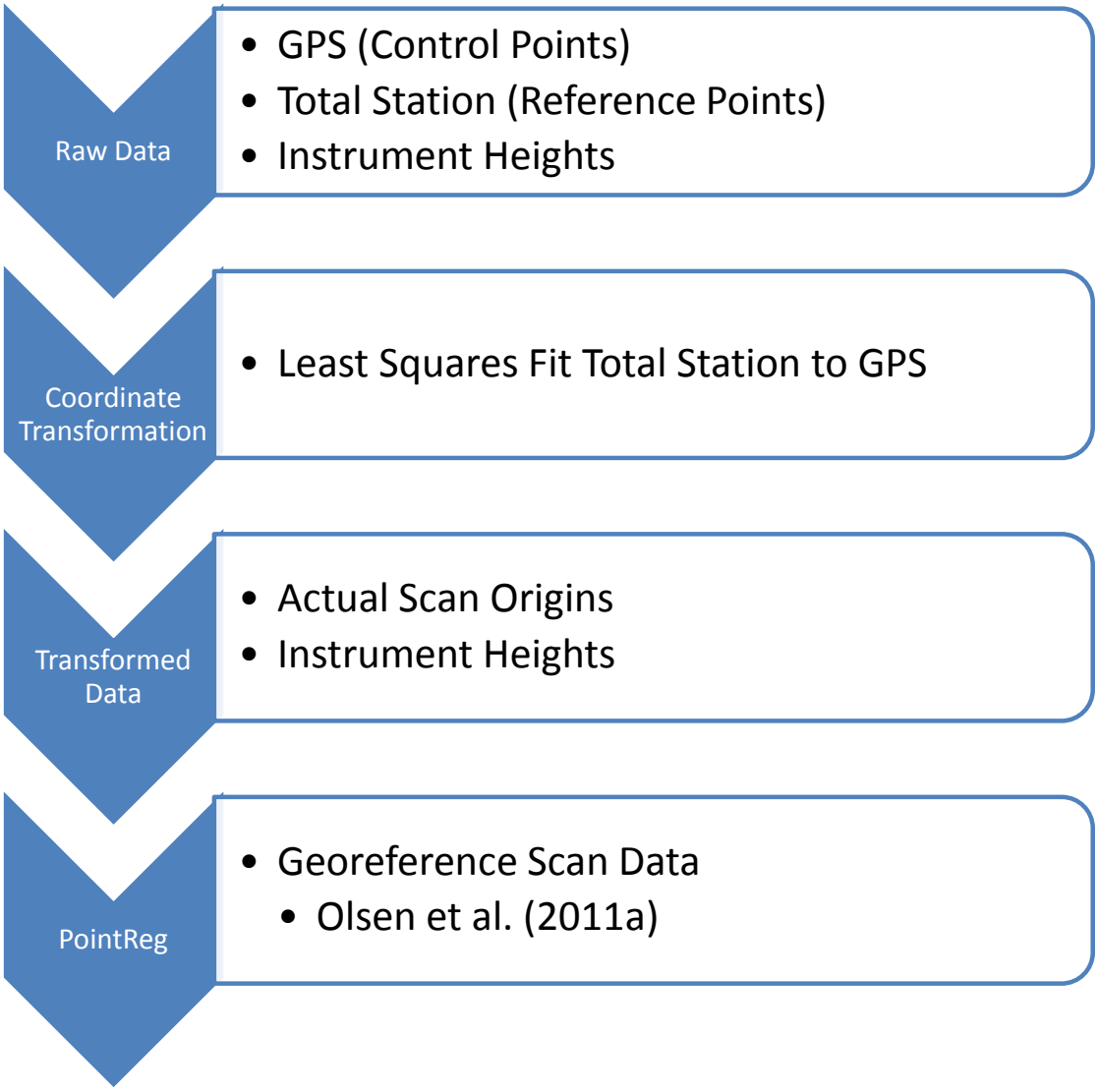

Figure 3-4 Flow diagram for the procedures for georeferencing data.

3.4.3 Create Tiles

Once the scans are geo-referenced, the "Tile Creator" divides the scan data into tiles if there are too many points in the entire dataset to create a DTM of the whole test site at one time due to memory constraints. It first calculates

the extents of the area to filter by using the coordinates for each scan origin, buffered by a predetermined scanner range distance, r_f, to which the scans will be filtered. For the JCL site, the filtered area was evenly divided into segments along the Y direction into tiles of equal area. Each data point is read in one by one and written out to the file associated with the specific tile. If a point is outside the filtered area it is no longer used. For this case study, three tiles were used with a scanner range distance of 100 meters.

3.4.4 Create Digital Terrain Model

A digital terrain model (DTM) is then created for the data within each tile. The terrain model was created by using a statistical filtering algorithm called Bin 'N' Grid. Olsen (2011b) provides details about how the algorithm works and its capabilities to filter out vegetation to obtain the ground surface. By gridding the data in large cells of 2 meters by 2 meters, and finding the minimum elevation in each grid to represent the ground surface, most of the landslide area is represented as the ground surface without vegetation. (Note that this filtering process works very well for airborne laser scans, but can have problems for small cell sizes (<10 cm) using terrestrial laser scans in dense forests due to the variability in point density and look angle.) The surface models created for each tile are then merged together to form a continuous DTM of the entire landslide area. A highly detailed DTM is not

required for the horizontal displacement evaluated in this study, but could provide vertical displacement information for the landslide.

3.4.5 Extract Slice Above Surface

The “Slice” extracts a thin slice of point cloud data at a specific height, *h*, above the DTM (Figure 3-5). The purpose of extracting a slice of data is to isolate individual trees and minimize the noise (points not actually on the tree trunks). Hence, the slice ideally should be taken above shrubs and other short vegetation on the ground, but also below the canopy. However, to minimize rotational effects and wind-induced displacements, the slice needs to be as close to the ground as possible. The points are filtered to satisfy the following criteria.

$$h - \Delta h < (h_i = z_i - z_{DTM}) < h + \Delta h \qquad (3.1)$$

Where:

h = height above DTM = 2.5 m for this study

Δh = 0.5 * slice thickness = 0.05 m for this study

h_i = height of point i,

z_i = elevation of point i, and

z_{DTM} = elevation on DTM at point i

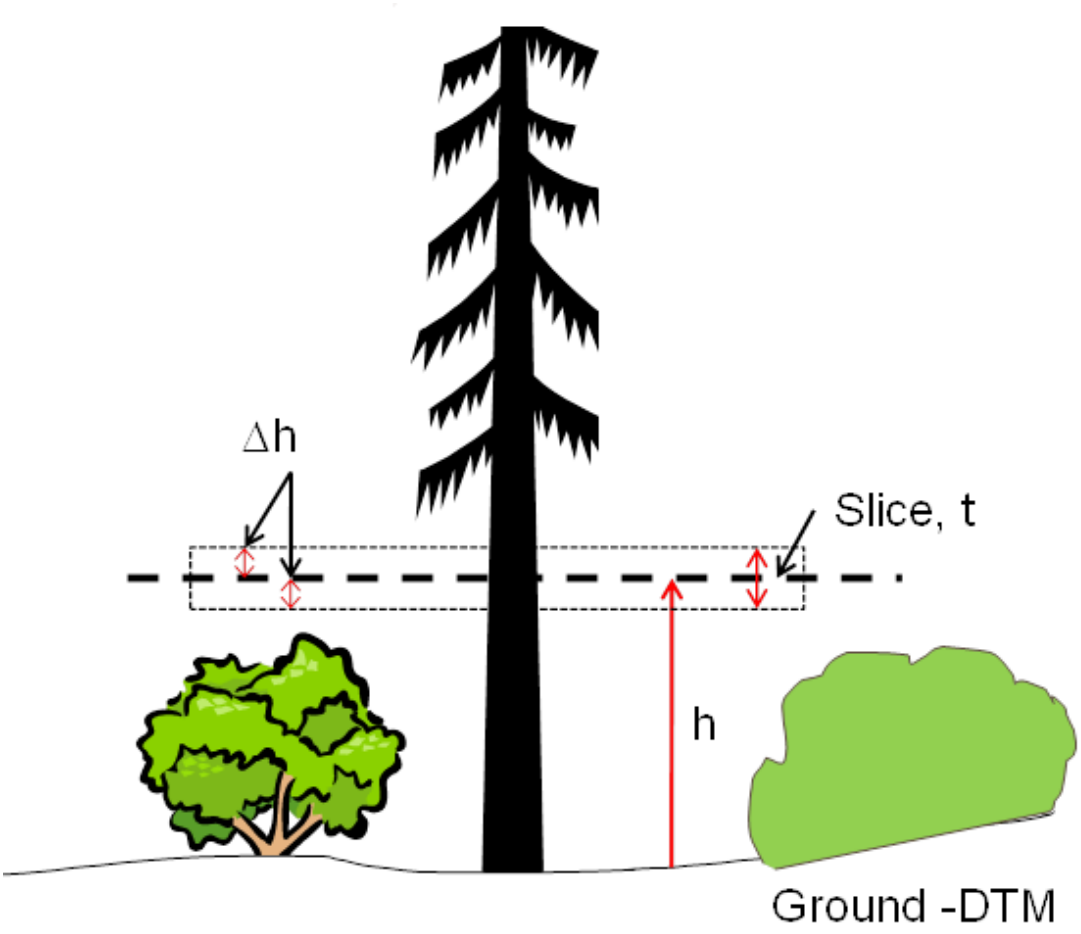

Figure 3-5 Example tree in the dataset illustrating the slice taken within the dashed rectangle.

3.4.6 Fit Circles to Trees

The “Trees” function searches through the “Slice” data to locate and fit circles to trees. It first reads in the “Slice” data and determines the extents of the dataset, which is then used to generate a hash table (organizational structure to enable efficient searching) based each point’s location within a grid. Initially, the grid is set up using the minimum and maximum values of the

X and Y coordinates as the extents of the grid. The cell size, Δ, within the grid is equal to the typical tree radius, r_{typ}. After the grid is established, each point from the dataset is indexed into the appropriate grid cell. "Trees" systematically searches through the data in sets of nine grid cells, a center cell and all of its closest neighbors (Figure 3-6). The algorithm starts in the lower left corner of the grid and moves through each row in the column. Upon reaching the top, it proceeds with the column to the right. Within each set of nine grid cells the numbers of points are determined. When there are more than N_{min} points (70 for this dataset), 2D circles (ignoring Z values because the slice is thin) are created through the points using a least-squares fit to all the data points.

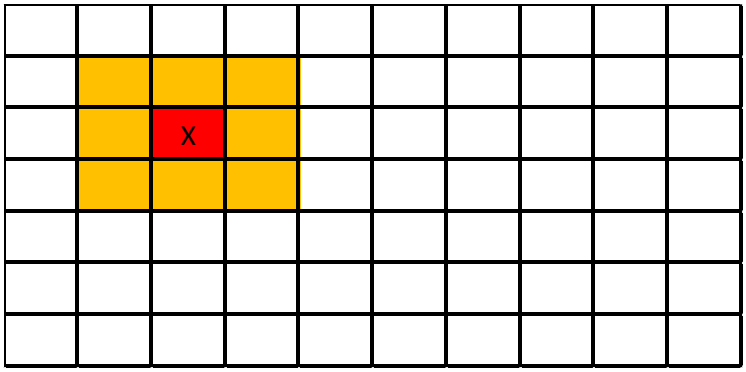

Figure 3-6 Example grid of dataset with the red grid cell is the center grid and the orange grid cells are the closest neighbors.

The initial circle is determined in a local coordinate system (u, v) by subtracting the averages, ẋ and ẏ, from x and y for each point. The center of

circle (u_c, v_c) is determined by minimizing the summation of residuals, S, in equation 3.2 (Bullock, 2006). The residuals are determined by taking partial derivatives with respect to S and setting it equal to zero, resulting in the best fit circle using equation 3.3. Then, converting back to the original coordinate system, the center of the circle (X_c, Y_c) = (u_c, v_c) + ($\dot{x}$, $\dot{y}$).

$$S = \sum_i \left((u_i - u_c)^2 + (v_i - v_c)^2 - r^2 \right)^2 \tag{3.2}$$

$$\begin{pmatrix} S_{uu} & S_{uv} \\ S_{uv} & S_{vv} \end{pmatrix} \begin{pmatrix} u_c \\ v_c \end{pmatrix} = \begin{pmatrix} 0.5(S_{uuu} + S_{uvv}) \\ 0.5(S_{vvv} + S_{vuu}) \end{pmatrix} \tag{3.3}$$

where:

$S_{uu} = \sum_i u_i^2$, $S_{uv} = \sum_i u_i * v_i$, $S_{vv} = \sum_i v_i^2$

$S_{uuu} = \sum_i u_i^3$, $S_{vvv} = \sum_i v_i^3$, $S_{uvv} = \sum_i u_i * v_i * v_i$, $S_{vuu} = \sum_i v_i * u_i * u_i$

The X and Y coordinates for the center of the circle (X_c, Y_c) and the radius, r, are then calculated as the parameters of the best fit circle. The root mean square error (RMS) of the input points to the circle fit can be calculated. Each point is examined individually and if the point is not within r $\pm$ 2 x RMS, it is marked as an outlier for the next iteration. The fitting process is then reiterated until the RMS of the fit is deemed acceptable by a user defined

threshold (1.5 cm recommended for this study) and outliers are removed. The final circle is then only used if (X_c, Y_c) are located within the center grid cell to avoid redundancy and ensure an optimal fit.

3.4.7 Compare Tree Locations Between Surveys

Following fitting circles to the tree trunk cross-section, the estimated displacement of the trees is measured by comparing the center of the circles between two surveys. The tree locations and radii for all the trees in both surveys are read by the "movement" program. "Movement" looks at each tree from the first survey and finds the closest tree to it from the second survey, within the same grid cell or its nearest neighbor grid cell. The radii of the two trees are compared (Δr) to ensure the two trees are reasonably the same tree, $\pm$ 1-5 cm, depending on user preference. After it is determined the two trees are likely the same tree, the horizontal displacement, δ, is determined with directional components: δ_X and δ_y, and total horizontal displacement, δ_{XY}. A file containing the X_c, $_{Yc}$, Z_c, r, N_{min} (the number of points used for the circle fit), and the RMS fit for each circle fit as well as $\delta_{X,}$ δ_y, and δ_{XY} is written.

3.4.8 Assumptions and Limitations

While this algorithm can detect the movement of the tree trunks, there are several assumptions and limitations to consider:

- the tree trunks can be modeled as circles with minimal error (RMS < 1.5 cm). In many cases, trees do not grow completely vertical, so if a large cross-section is used, an ellipse may be required.
- the tree's best fit circle occurs when its coordinates are located in the center grid, rather than a neighbor grid.
- trees are spaced, *s*, farther apart than at least 1.5 times the typical tree diameter, *d*. In other words, trees are not too close together.
- the displacement, δ, is less than cell size, Δ. This requires good temporal resolution to trace the paths of trees; with significant time, movement may exceed the cell size, Δ.
- the landslide is only monitored at the surface; no subsurface information is obtained. Further, if there is a significant rotation component to the landslide, the technique may overestimate landslide translational displacement if circles are not extracted close to the ground.

3.5 RESULTS AND DISCUSSION

3.5.1 Landslide Movement Across Slide

The algorithm was applied to JCL to test its effectiveness in determining landslide movement, including distinguishing variable movement across the slide. To estimate the amount of landslide movement taking place,

coordinates for the center of the trees were compared between consecutive surveys. Negative δx values indicate movement to the west and positive values indicate movement east. Positive δy values indicate movement north and negative values indicate movement south.

Figure 3-7 shows the landslide movement between April 2012 and November 2012 surveys. The majority of the trees show movement between 6 and 14 cm. The area with the greatest amount of movement is located on the western side of the landslide near the bluff face. Trees were defined with expected results when: $-0.14 < \delta x$ (m) < 0, $-0.1 < \delta y$ (m) < 0, and $0.15 \leq \delta xy$ (m). For the 71 trees detected at h = 2.5 m, RMS $\leq$ 1.5 cm and $\Delta r \leq$ 5 cm, 93% of the trees have expected results. These trees provide the capability to monitor more locations than are typically monitored through traditional methods for this site, enabling quantification across more of the landslide area. Figure 3-8 interpolates the movement at unmeasured locations by using an inverse distance weighted (IDW) technique to determine the value of each pixel using the five closest trees and weighting them according to the distance from the pixel. Within the landslide, smaller blocks with increased or decreased movement are detected. For example, Figure 3-8 shows a block next to the sea cliff that is advancing at a faster rate than the rest of the landslide along the sea cliff; there is also a clear break line at the southern end of the landslide, where there should be no movement.

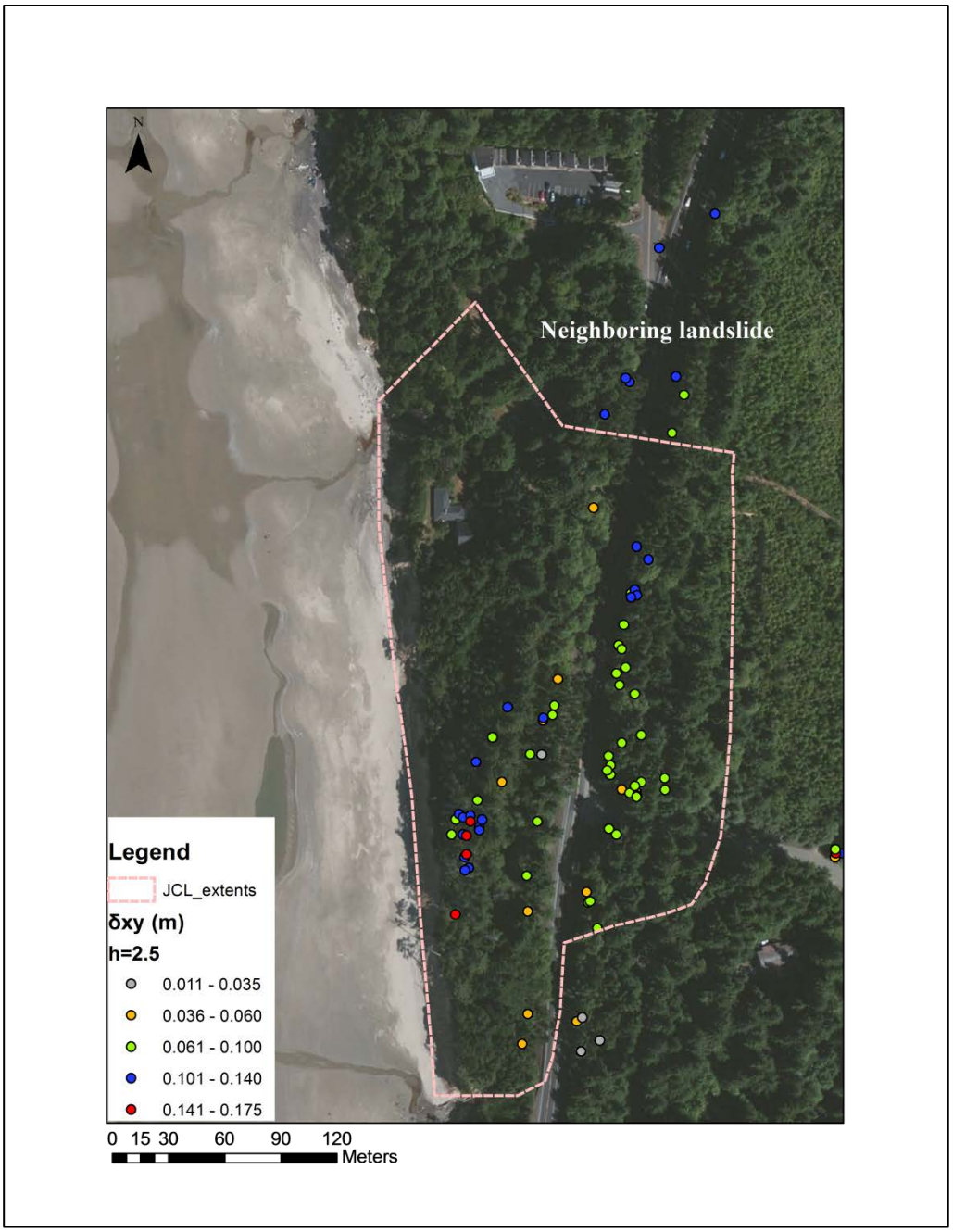

Figure 3-7 Landslide total displacement, δxy. Base map photographs provided by ESRI.

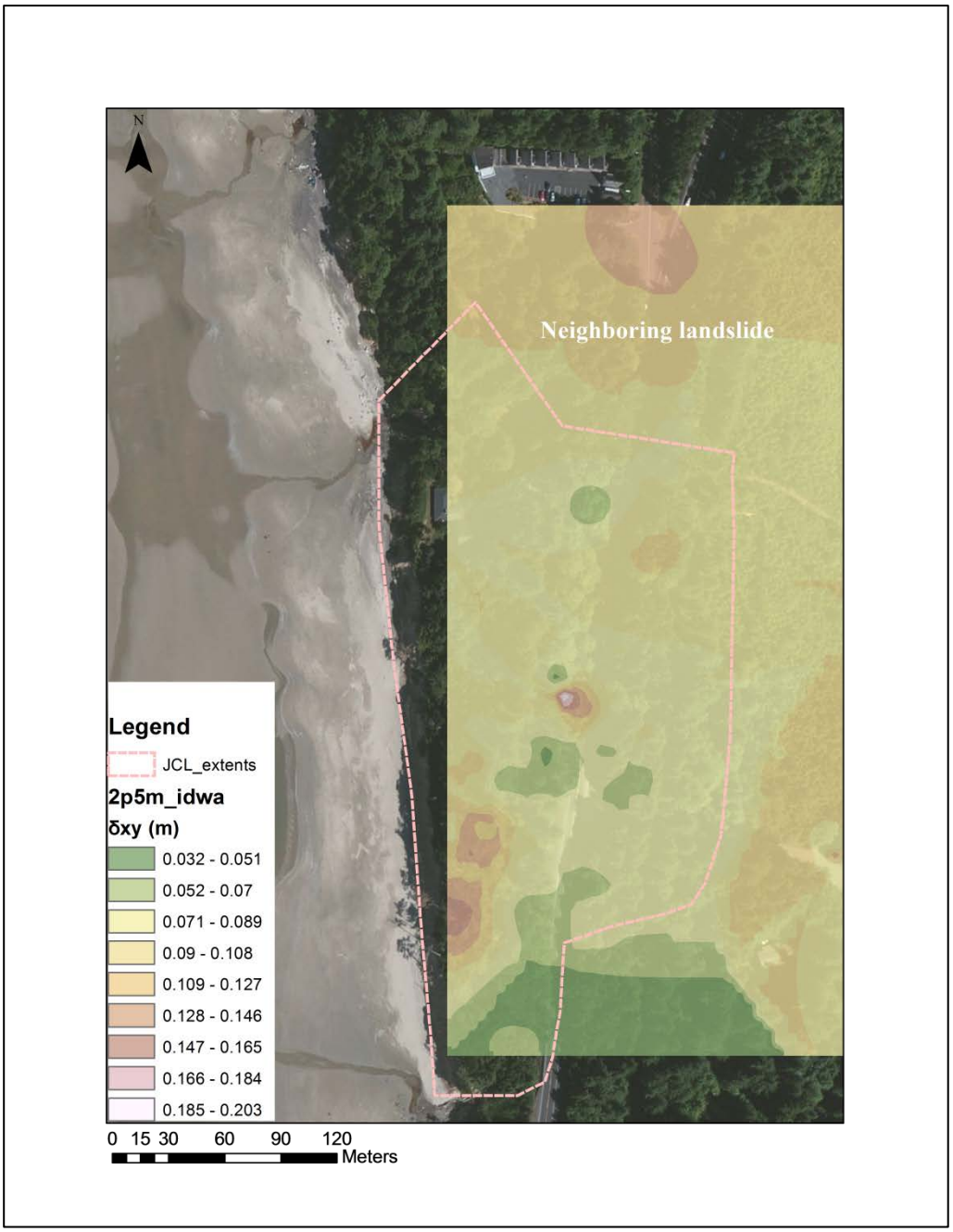

Figure 3-8 Map of JCL interpolating movement from neighboring trees. Base map photographs provided by ESRI.

3.5.2 Erosion on Bluff Face

Figure 3-9 shows the results of a change analysis of a triangulated surface model (created using the surfacing method described in Olsen et al. 2013) of the bluff face between April 2012 and November 2012, with differences up to 50 cm. For this analysis, the April 2012 model was used as the base survey when compared to the November 2012 survey. The negative numbers are shown in orange and represent a retreat from the ocean due to erosion exceeding landslide movement. Positive numbers are shown in blue and represent advancement toward the ocean (landslide movement and accretion exceeds erosion) and green represents values exceeding the 50 cm threshold. In general, the upper slopes of the bluff face have retreated from subaerial mechanisms (e.g. precipitation). The advancement at the base of the cliff is buildup of talus deposits from the eroded material above.

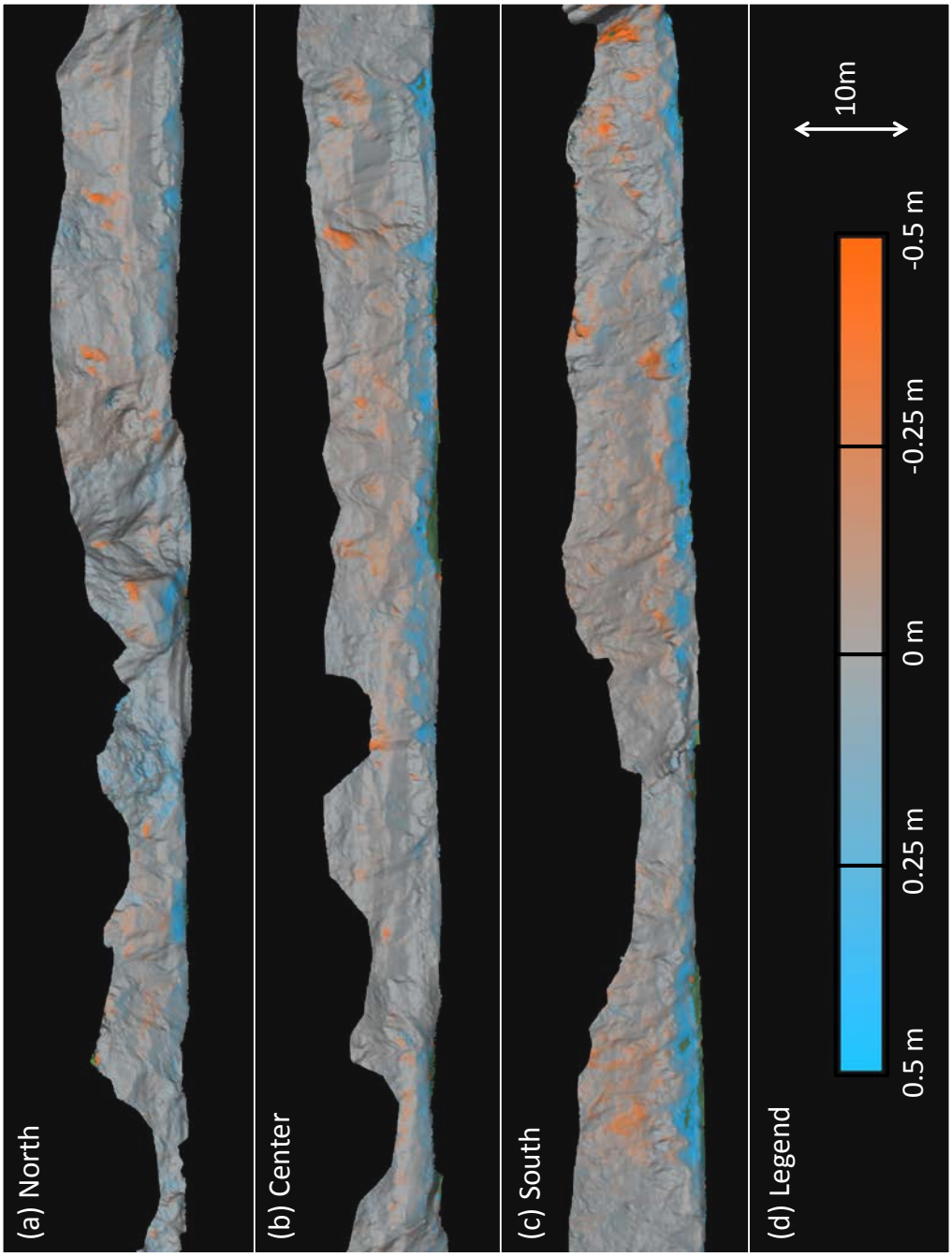

Figure 3-9 Change analysis between laser scan surveys showing advance (landslide movement, accretion) and retreat (erosion) of the cliff face between April 2012 and November 2012.

3.5.3 Validation

For the surveys conducted at JCL, the uncertainty of the tree movement determined by this new technique was evaluated by comparing the movement at 10 points using traditional surveying techniques, based on the same RTK control, to the movement of the closest valid tree (Table 3-1). Five additional points were initially set, but destroyed between surveys (from road re-surfacing), preventing comparison. The results show that the average differences in the amount of movement calculated for $\delta_{X,}$ δ_{y}, and δ_{XY} are 1.7, 1.8 and 1.4 cm with a standard deviation of $\pm$ 1.5, 1.3, and 1.2 cm respectively. These fall within the anticipated error budget of the total station network tied to RTK GPS control points. The largest error is in the GPS control points, followed by the total station network. The next largest sources of error is in the process of fitting circles to a cross-section of data to represent tree trunks.

Table 3-1 Compared displacement of total station and GPS network to closest tree.

Conventional survey				Closest tree			Absolute Difference			Distance from tree (m)
Point	δx (m)	δy (m)	δxy (m)	δx (m)	δy (m)	δxy (m)	δx (m)	δy (m)	δxy (m)	
14	-0.067	-0.036	0.076	-0.082	-0.028	0.087	0.015	0.008	0.011	16
15	-0.056	-0.042	0.070	-0.053	-0.025	0.059	0.003	0.017	0.011	9
16	-0.081	-0.036	0.089	-0.083	-0.039	0.092	0.002	0.003	0.004	12
18	-0.082	-0.050	0.096	-0.045	-0.039	0.060	0.037	0.011	0.036	7
19	-0.107	-0.038	0.114	-0.091	-0.053	0.105	0.016	0.015	0.009	10
20	-0.129	-0.034	0.133	-0.135	-0.034	0.139	0.006	0.000	0.006	3
22	-0.082	-0.037	0.090	-0.085	-0.007	0.085	0.003	0.030	0.005	11
23	-0.082	-0.021	0.085	-0.118	-0.025	0.121	0.036	0.005	0.036	7
24	-0.105	-0.024	0.108	-0.105	-0.039	0.112	0.000	0.015	0.004	16
25	-0.122	-0.059	0.135	-0.146	-0.015	0.147	0.024	0.044	0.012	3

Max	0.037	0.044	0.036
Min	0.000	0.000	0.004
Average	**0.017**	**0.018**	**0.014**
Std dev	**0.015**	**0.013**	**0.012**

Figure 3-10 shows the comparison of a segment of the point clouds near the bluff face between April 2012 and November 2012 using "CloudCompare", an open source software (DGM, AB, & RM, 2012). The comparison shows the distances between the closest points in each point cloud. The points on the ground are noise with no consistent movement detection. The movement shown throughout most of the middle of the tree is fairly steady ranging from 11 to 20 cm of movement. This is also consistent with the displacement measure through conventional survey and its closest tree at point 25. Point 25 is the closest conventional survey point to this tree. Although this software shows detailed change, it is difficult to represent the movement of individual

trees shown with a single value across a large area. Further, because the method looks for closest points and does not actually track the same points, it will under predict change on the sides of the trees perpendicular to the movement, as shown in the figure.

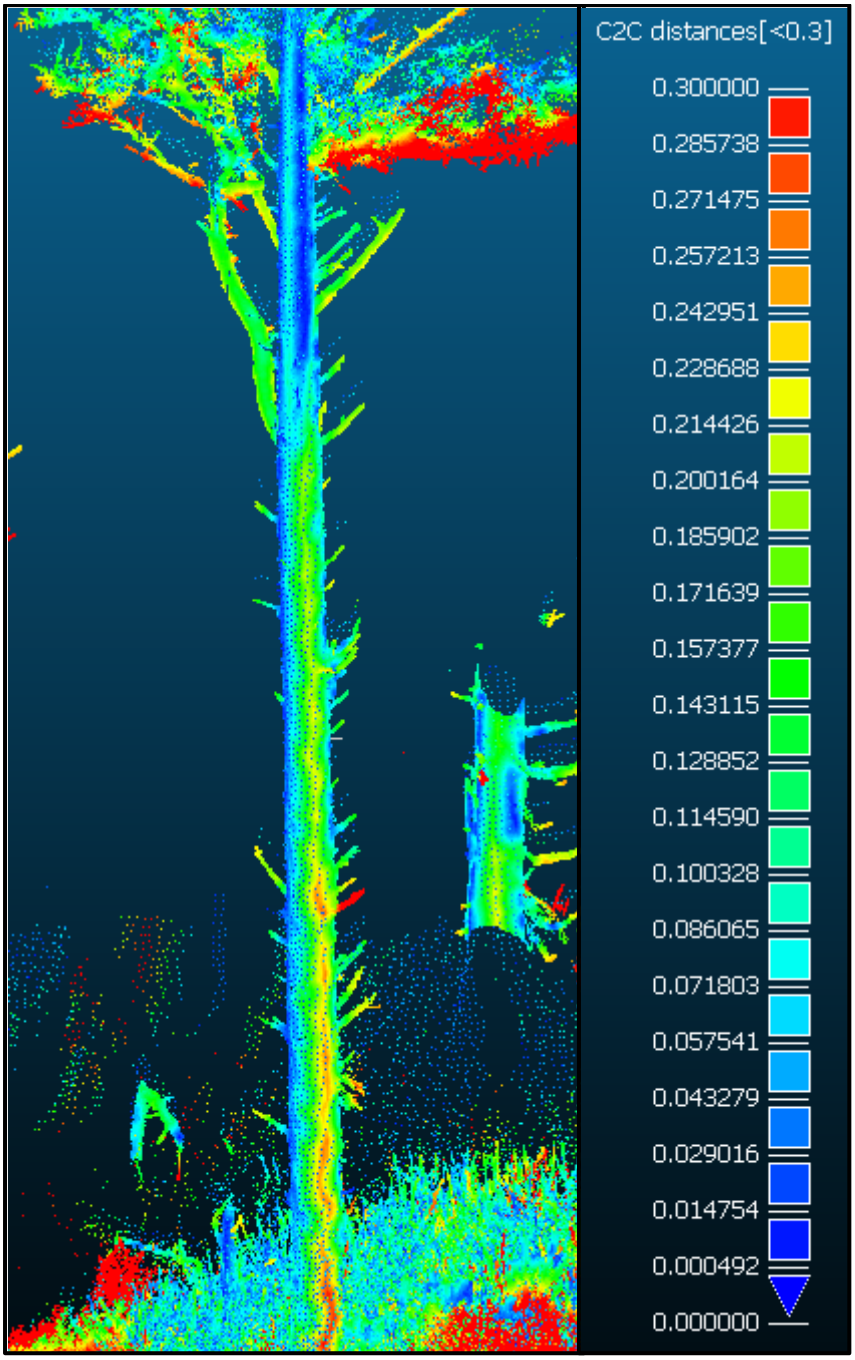

Figure 3-10 Point cloud compared between laser scan surveys showing movement (m) of the trees between April 2012 and November 2012.

3.5.4 Parametric Analysis

Selecting the appropriate height above the DTM, *h*, to take a slice of data, *t*, and an acceptable RMS value for the circle fit is a balance between pairing enough trees and rejecting false tree pairings and poor circle fits. The height above the DTM for the slice is highly dependent on the type and variability of vegetation in the forested area and canopy of the trees. Figure 3-11 to Figure 3-18 show the relationship between the number of trees detected, *M*, circle fit RMS for the trees, and the reliability of the trees for various Δr curves and with different *h* values. Reliability was determined by dividing the number of trees with expected results by the total number of trees. As the acceptable RMS value increases, more trees are paired together, but the reliability of the trees decrease. When a slice of data is taken within the vegetation (*h* = 2.0 m) fewer trees are paired at low RMS values. As the RMS value increases, the reliability of the trees rapidly decreases. With high *h* values (6.0 m), when the slice is in the canopy of the trees, the reliability of the trees is about 5% lower than a slice taken between the vegetation and the canopy (h = 2.5 m or 4 m). For all cases above the vegetation the number of trees identified increases significantly when using a RMS threshold value between 0.5 to 1.0 cm. After a RMS value of 1.5 cm, the number of trees starts to level off and few additional trees are found. The Δr parameter produces the largest increase in the number of trees when increased from 0.5

cm to 1.0 cm, with the lowest impact on reliability. Optimal use, providing the most trees with the highest level of reliability, is where both curves start to level off, which is at a RMS value of 1.5 cm and a Δr value of 1.0 cm. Using the optimal parameters provides more monitoring locations (reliable trees) than typically obtained using current methods for all h values.

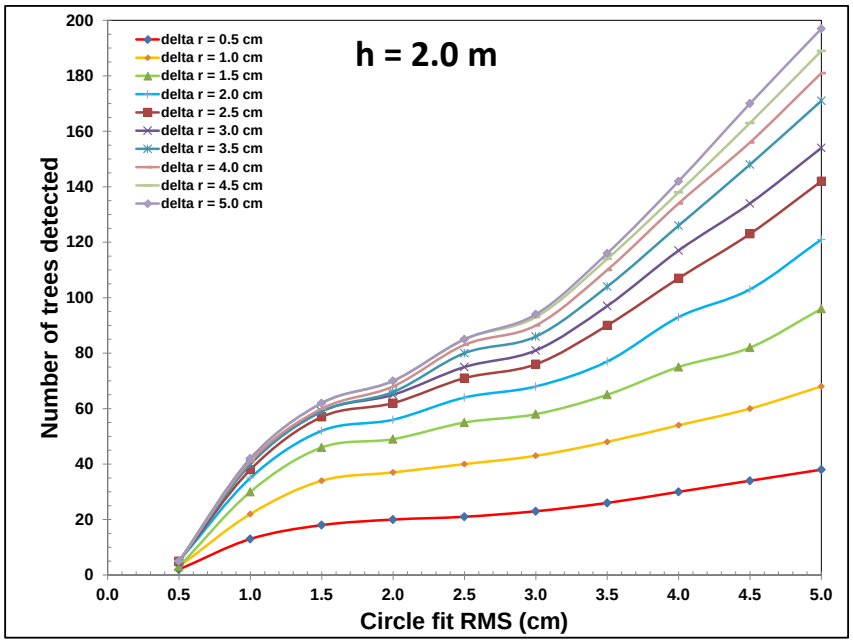

Figure 3-11 Number of trees detected at 2.0 m above DTM based on circle fit RMS for various Δr curves.

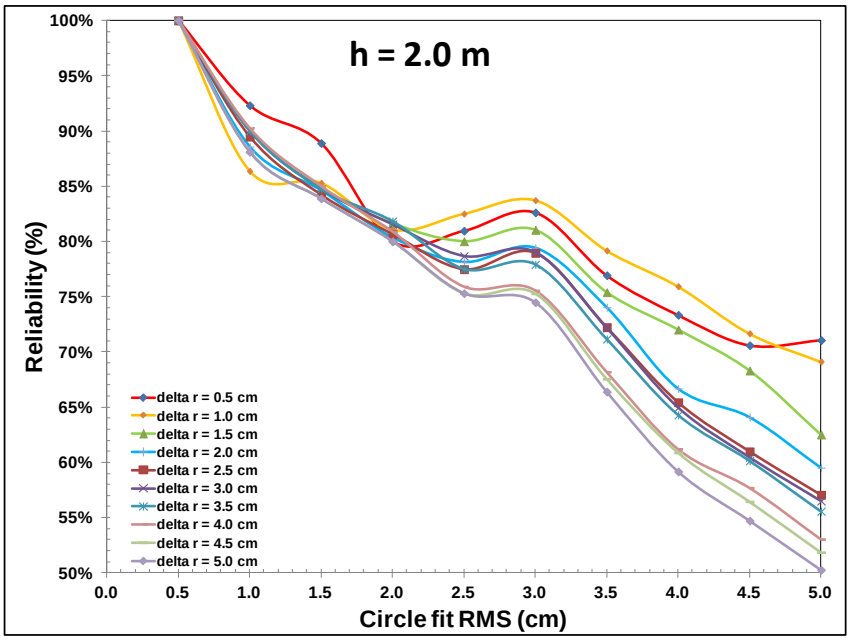

Figure 3-12 Reliability of trees detected at 2.0 m above DTM based on circle fit RMS for various Δr curves.

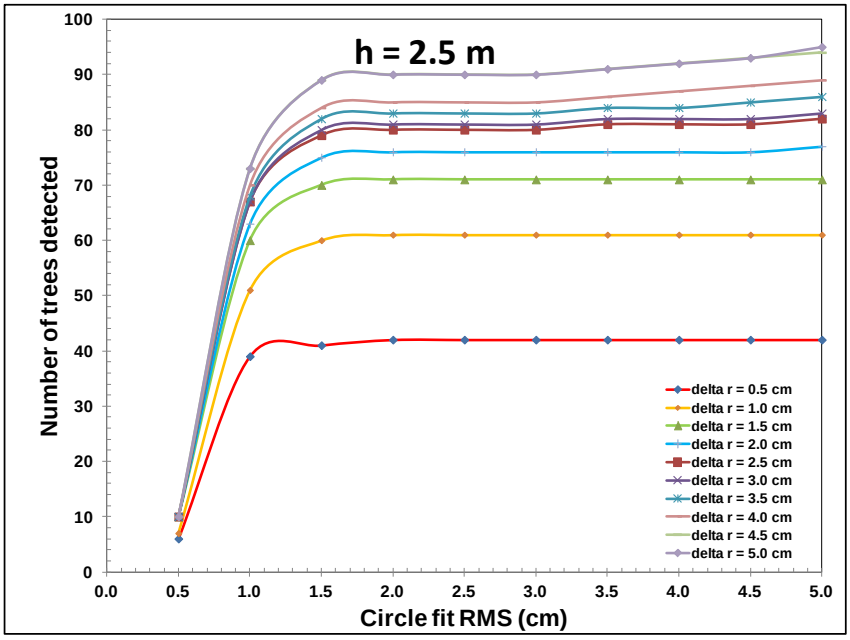

Figure 3-13 Number of trees detected at 2.5 m above DTM based on circle fit RMS for various Δr curves.

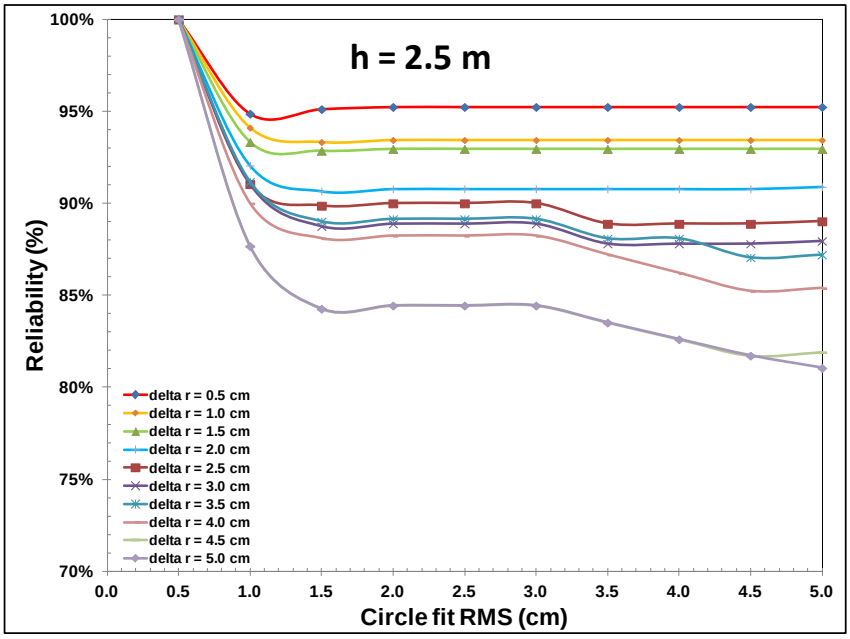

Figure 3-14 Reliability of trees detected at 2.5 m above DTM based on circle fit RMS for various Δr curves.

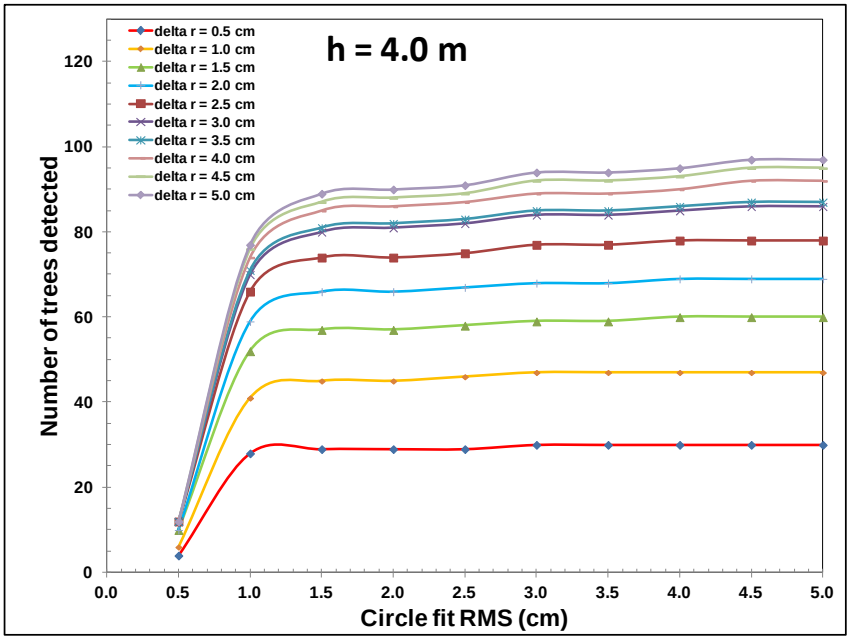

Figure 3-15 Number of trees detected at 4.0 m above DTM based on circle fit RMS for various Δr curves.

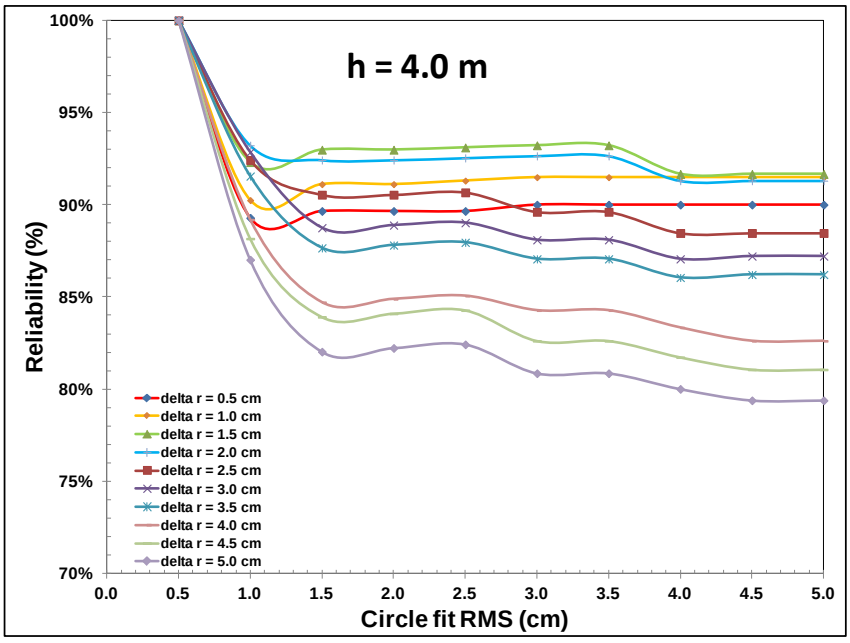

Figure 3-16 Reliability of trees detected at 4.0 m above DTM based on circle fit RMS for various Δr curves.

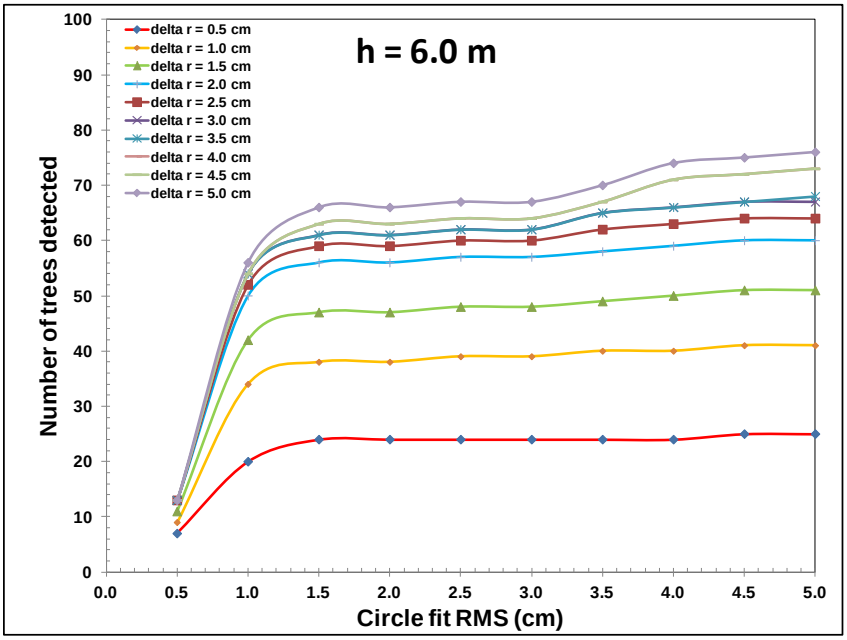

Figure 3-17 Number of trees detected at 6.0 m above DTM based on circle fit RMS for various Δr curves.

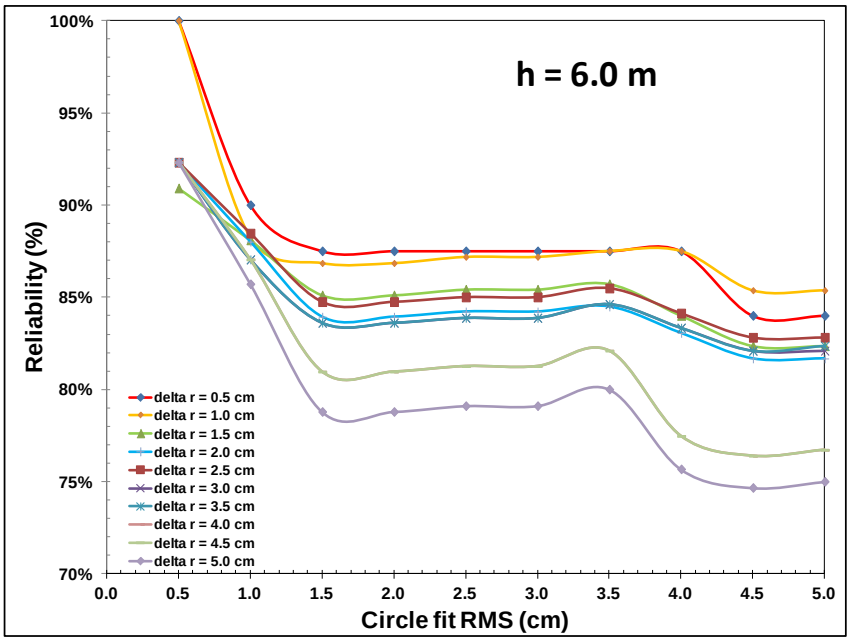

Figure 3-18 Reliability of trees detected at 6.0 m above DTM based on circle fit RMS for various Δr curves.

3.5.5 Time Analyses

The time this methodology takes to determine movement for a landslide will vary based on the number of trees and the size of the datasets. However, for this case study (~ 700 million data points per survey), using an Intel(R) Xeon(R) quad-core CPU with a 64-bit operating system, 24 GB RAM and solid state hard drives, it took about 20 minutes to tile the data. Generating the DTM for the test site took about 15 minutes and extracting a slice from both datasets took about 15 minutes. Finding trees took less than 10 minutes and comparing the location of the trees took less than a minute. Overall, after the data was processed this methodology shows landslide displacement results in about one hour, which is mostly computer processing time for the algorithm rather than user input.

3.6 CONCLUSION

By using natural features such as trees to monitor landslide movement, TLS surveys can efficiently model landslide movement over the entire landslide area (Figure 3-8). The method detailed in this paper demonstrates TLS surveys of natural features in a forested environment can quantify landslide displacement, consistent with traditional survey devices. The JCL shows displacements of 6 cm to 14 cm throughout most of the landslide area. It is also important to collect data outside the extents of the test site to validate

the methodology and determine the impacts the landslide movement has on surrounding landmass. For example, Figure 3-7 shows just outside the southern extent of the landslide the trees are not moving with the landslide, but they are still affected with movement. It has not only been shown that landslide movement can be detected, but that the quality of the modeled displacement depends on the RMS of the circle fit and the difference in the radii of trees between surveys. Understanding how these parameters affect the quality of the tree paring will allow researchers to accurately model landslide movement in forested environments. Although the optimal parameters for JCL are a RMS value less than 1.5 cm and radii difference less than 1.0 cm, this will change based on each forested area. Therefore, it is recommended users implement a similar analysis to determine their optimal parameters for their study area.

While this is a short term study, this research paves the way for additional work in understanding long term trends using the automated, systematic methodology presented herein. Further research should be conducted to analyze the mechanics of the landslide similar to Figure 3-8. Now that a baseline for the entire JCL has been established, future TLS can be used to evaluate the seasonal effects and longer term movement rates of this landslide. Finally, extracting two slices at different heights may assist in determining if there is a large rotational component to the landslide.

3.7 ACKNOWLEDGEMENTS

The authors would like to thank Leica Geosystems, David Evans & Associates, and Maptek I-Site for providing the equipment and software used for this research. Additionally, Oregon Department of Transportation provided travel support for field work. Thank you to Jonathan Allan and George Priest for a thorough Johnson Creek Landslide site visit physically showing and explaining previous work done and the geological setting. Thank you to Keith Williams, Rubini Mahalingam, and John Raugust for assistance with data collection.

4 OVERALL CONCLUSION

This research has studied the use of terrestrial laser scanning to monitor coastal landslide movement in a forested area. Terrestrial laser scanning systems provide the capability to detect and monitor coastal landslide movement in forested areas with greater spatial and temporal resolution than current conventional techniques. The automated method of using tree trunks to extract landslide movement provides data throughout the entire landslide area, showing variability across the slide. Being able to use natural features to monitor landslide movement produced more monitoring locations, with reliable displacements than typically monitored using conventional methods. A parametric analysis of the methodology revealed that the optimal parameters for JCL were a circle RMS less than 1.5 cm and Δr less than 1.0 cm at a height of 2.5 m above the DTM. Although these were the optimal parameters for JCL they are highly dependent on the surrounding vegetation and canopy cover, so researchers should conduct similar analysis when using this methodology to determine the optimal parameters for their test site for best results.

The methodology presented within this document lays the groundwork for a wide range of additional research. The results have potential to be misinterpreted due to inaccurate GPS readings or misalignment, but because

the validation uses the same control points the methodology is still valid. This methodology enables researchers to separate landslide movement from the active erosion in dynamic coastal environments, such as Johnson Creek Landslide, allowing improved volumetric sediment contributions to the littoral system. This can assist in monitoring long term trends and movement rates within a landslide. Further, this methodology allows detailed landslide monitoring to detect and analyze the mechanics or variable block movements within a landslide. This methodology can also be extended to extract ellipses instead of circles to represent cross-sections of tree trunks to provide additional data about the trees. Furthermore, the results of the tree displacement could be validated by an external remote sensing technique such as ground based radar.

While this methodology is applied to landslide movement for this research, it could be used for many other applications as well. City departments could use this to monitor tree growth in urban areas by monitoring tree radius growth over time. Also, it could be used in the forestry profession could use this methodology to inventory plots or any other aspect of tree inventory.

5 WORKS CITED

Buckley, S. J., Vallet, J., Braathen, A., & Wheeler, W. (2008). Oblique Helicopter-Based Laser Scanning For Digital Terrain Modelling and Visualisation of Geological Outcrops. *The International Archives of the Photogrammetry, Remote Sensing and Spatial Information Sciences, 37(4)*, 493-498.

Bullock, R. (2006). *Least-Squares Circle Fit*. Retrieved from http://www.dtcenter.org/met/users/docs/write_ups/circle_fit.pdf

Burns, W. J., & Madin, I. P. (2009). *Protocol for inventory mapping of landslide deposits from light detection and ranging (LIDAR) imagery.* DOGAMI, Special Paper 42.

Collins, B. D., & Stock, G. M. (2012). Lidar-based rock-fall hazard characterization of cliffs. *GeoCongress 2012* (pp. 3021-3030). American Society of Civil Engineers.

Collins, B., & Sittar, N. (2008). Processes of coastal bluff erosion in weakly lithified sands, Pacifica, California, USA. *Geomorphology, 97*, 483-501.

DGM, AB, & RM. (2012, 11 30). *CloudCompare*. Retrieved 03 10, 2013, from CloudCompare: http://www.danielgm.net/cc/

Dunning, S., Rosser, N., & Massey, C. (2010). The integration of terrestrial laser scanning and numerical modelling in landslide investigations. *Quarterly Journal of Engineering Geology and Hydrogeology, 43*, 233 - 247.

Fernandez Merodo, J., Pastor, M., Mira, P., Tonni, L., Herreros, M., Gonzalez, E., & Tamagnini, R. (2004). Modelling of diffuse failure mechanisms for catastrophic landslides. *Comput. Methods Appl. Mech. Engrg. 193*, 2911-2939.

GIM International. (2011, February). *Airborne Lidar Scanners: GIM International*. Retrieved July 30, 2012, from GIM Internation: http://www.gim-international.com/productsurvey/id44-Airborne_Lidar_Scanners,_February.html

Interactive Software Designs. (2011). *XSTABL*. (Interactive Software Designs) Retrieved 03 07, 2013, from http://www.xstabl.com/

Intergovernmental Panel on Climate Change. (2007). *Climate Change 2007 - The Physical Scenece Basis.* Paris.

Jaboyedoff, M., Oppikofer, T., Abellan, A., Derron, M.-H., Loye, A., Metzger, R., & Pedrazzini, A. (2012). Use of LIDAR in landslide investigations: a review. *Natural Hazards*, 61: 5-28.

Komar, P. D. (1998). *The Pacific Northwest Coast: Living with the Shores of Oregon and Washington.*

Landslide Technology. (2004). *Geotechnical investigation Johnson Creek Landslide, Lincoln County, Oregon.* DOGAMI Open-File Report O-04-5, 115 p.

Lehtomaki, M., Jaakkola, A., Hyypppa, J., Kukko, A., & Kaartinen, H. (2011). Performance Analysis of a Pole and Tree Trunk Detection Method for Mobile Laser Scanning Data. *ISPRS Workshop Laser Scanning*, *XXXVIII-5/W12.* Calgary, Canada.

Lemmens, M. (2010, August). *Terrestrial Laser Scanners: GIM International*. Retrieved July 30, 2012, from GIM International: http://www.gim-international.com

Mitchell, C. E., Vincent, P., Wedlon II, R., & Richards, M. (1994). Present-day vertical deformation of the Cascadia margin, Pacific Northwest, United States. *Journal of Geophysical Research*, Vol 99(B6), 12,257-12,277.

North, W., & Byrne, J. (1965). *Coastal Landslides of Northern Oregon.* The Ore Bin 27 (11), 217-241.

Olsen, M. (2011b). *Bin 'N' Grid: A simple program for statistical filtering of point cloud data*. Retrieved 03 05, 2012, from LiDAR News: http://www.lidarnews.com/content/view/8444/208/

Olsen, M. J., Johnstone, E., Kuester, F., Driscoll, N., & Ashford, S. A. (2011a). New Automated Point-Cloud Alignment for Groud-Based Light Detection and Ranging Data of Long Coastal Sections. *Journal of Surveying Engineering, 137*, 14-25.

Olsen, M. J., Kuester, F., & Johnstone, E. (2013). Hinged, pseudo-grid triangulation method for long, near-linear cliff analyses. *Journal of Surveying Engineering, 139*(2), 105-109.

Olsen, M., Allan, J., & Priest, G. (2012a). Movement and erosion quantification of Johnson Creek, Oregon landslide through 3D laser scanning. 10.

Olsen, M., Butcher, S., & Silvia, E. (2012b). *Real-time change and damage detection of landslides and other earth movements threatening public infrastructure.* OTREC Final Report 2011-23 and ODOT Final Report SR 500-500.

Olsen, M., Johnstone, E., Driscoll, N., Ashford, S., & Duester, F. (2009). Terrestrial laser scanning of extended cliff sections in dynamic environments: a parameter analysis. *J. of Surveying Enginerring, ASCE, 135 (4)*, 161-169.

Priest, G. R., Allen, J. C., Niem, A., Christie, S. R., & Dickenson, S. E. (2006). *Interim report: Johnson Creek landslide project.* Lincoln County, Oregon: Oregon Department of Geology and Mineral Industries, 184 p.

Priest, G. R., Schulz, W. H., Ellis, W. L., Allan, J. A., Niem, A. R., & Niem, W. A. (2011). Landslide Stability: Role of Rainfall-Induced, Laterally Propagating, Pore-Pressure Waves. *Environmental & Engineering Geoscience, XVII (4)*, 315 - 335.

Priest, G., & Allan, J. (2004). *Evaluation of coastal erosion hazard zones along Dune and Bluff backed shorelines in Lincoln County, Oregon: Cascade Head to Seal Rock.* Oregon Department of Geology and Mineral Industries, Open File Report O-04-09, Portland, OR.

Priest, G., Allan, J., Niem, W., & Kickenson, S. (2008). *Johnson Creek Landslide Research Project, Lincoln County, Oregon.* DOGAMI Special Paper 40.

Puente, I., Gonzalez-Jorge, H., Arias, P., & Armesto, J. (2011). Land-Based Mobile Laser Scanning Systems: A Review. *ISPRS Workshop Laser Scanning*, *XXXVIII-5/W12.* Calgary, Canada.

Renslow, M. (2012). *Manual of Airborne Topographic LIDAR.* ASPRS.

Rosen, P. A., Hensley, S., Joughin, I. R., K., L. F., Madsen, S. N., Rodriguez, E., & Goldstein, R. (2000). Synthetic Aperture Radar Interferometry. *IEEE, 88*(3), 333-382.

Rosser, N., Petley, D., Lim, M., Dunning, S., & Allison, R. (2005). Terrestrial laser scanning for monitoring the process of hard rock coastal cliff erosion. *Quarterly Journal of Engineering Geology & Hydrogeology, 38 (4)*, 363-375.

Schulz, W. H., & Ellis, W. L. (2007). *Preliminary Results of Subsurface Exploration and Monitoring at the Johnson Creek Landslide, Lincoln County, Oregon.* USGS Open-File Report 2007-1127, 11 p.

Schulz, W., Galloway, S., & Higgins, J. (2012). Evidence for earthquake triggering of large landslides in coastal Oregon, USA. *Geomorphology*, 88-98.

Vosselman, G., & Maas, H.-G. (2010). *Airborne and Terrestrial Laser Scanning* (North American ed.). Caithness, Scotland, UK: Whittles Publishing.

Wang, G. (2011). GPS Landslide Monitoring: Single Base vs. Network Solutions - A case study based on the Puerto Rico and Virgin Islands Permanent GPS Netwrok. *Journal of Geodetic Science*, 191-203.

Wehr, A., & Lohr, U. (1999). Airborne laser scanning—an introduction and overview. *ISPRS Journal of Photogrammetry & Remote Sensing, 54*, 68-82.

Wieczorek, G. F., & Snyder, J. B. (2009). Monitoring slope movements. *The Geological Society of America*, 245-271.

Young, A. P., Guza, R., Flick, R., O'Reilly, W., & Gutierrez, R. (2009). Rain, waves, and short-term evolution of composite seacliffs in southern California. *Marine Geology, 267*(1-2), 1-7.

Young, Adam P., Olsen, M. J., Driscoll, N., Flick, R.E., Gutierrez, R., Guza, R.T., Johnstone, E., & Kuester, F. (2010). Comparison of Airborne and Terrestrial Lidar Estimates of Seacliff Erosion in Southern California. *J. of Photogrammetric Engrg. and Remote Sensing, ASPRS 76(4)*, 421-427.

APPENDICES

APPENDIX A – PROGRAM DETAILED PSEUDO CODE

1. **Tiles**, requires: csv file with scanner locations, .bov file with points, same file name
    a. Welcome to Tile program
    b. Asks user for minimum and maximum elevation to filter (elevations that contain the ground above the cliff)
    c. Stores the min and max elevation from user input
    d. Shows the user the filter range for elevation
    e. Reads in csv file (scanner locations): readcsvfile(char* csvfilename, XYZpt* &points, int &npts)
        i. Opens file
        ii. Counts points, **npts**
        iii. Stores points in memory as **points (.x, .y, .z, .id)**
        iv. Closes
    f. Prints csv points: printcsv(XYZpt* points, int npts)
        i. Prints x, y, z, and id for each csv point to make sure the right points are used for the tiles.
    g. Calculates the tiles for the dataset: calctiles(XYZpt* points, int npts)
        i. Calculates xmin from the csv file, **csvstats.xmin**
        ii. Calculates xmin from the csv file – scanner range (100m), **csvext.xmin**
        iii. Calculates xmax from the csv file, **csvstats.xmax**
        iv. Calculates xmax from the csv file + scanner range (100m), **csvext.xmax**
        v. Calculates ymin from the csv file, **csvstats.ymin**
        vi. Calculates ymin from the csv file – scanner range (100m), **csvext.ymin**
        vii. Calculates ymax from the csv file, **csvstats.ymax**
        viii. Calculates ymax from the csv file + scanner range (100m), **csvext.ymax**
        ix. Calculates the divisions in the y direction (**ydivs[i]**) based on the number of tiles (**ntiles**) desired by the user. Ntiles is currently hard coded to 3 tiles.
        x. Shows the user the y values for each tile
    h. Changes file extension: char* replaceextension(const char * filename, char* ext, bool stdext)

i. Creates a new file name with a different extension to create a new file extension .bov file instead of .csv file.

i. Creates tiles: readbin(const char* fname_in, unsigned long int &numpts, XYZpt &offset, double zmin, double zmax, double ydivs[])
   i. Reads in binary file
   ii. Creates and opens binary headers and files for each of 3 tiles (eg. _1h and _1) based on original bov file name.
   iii. Reads header file from original bov file determines offset.x, offset.y and offset.z.
      1. Without header file all offsets set to 0
      2. Writes offsets from original bov file to each of 3 tile header files
      3. Closes tile header files
      4. Displays offsets for the header files
   iv. Writes data into tile files
      1. Determines y divisions for each tile based on the offsets
      2. Reads in each point from .bov file
         a. Filters points outside user defined z min and z max values
         b. Writes points to appropriate binary file based on y divisions and offsets
         c. Closes the binary tile files
         d. Deletes points from memory
j. Tells the user the tiles are complete!

The 3 tile files are used in bin and grid to create a surface model of the landslide area. The 3 surface models are then merged together to make a complete surface model **resulting in one flt file.**

2. Slice, Requires: Flt and Hdr file for the surface model generated from bin and grid, bov file with points from
    a. Welcome to the slice creator
    b. Creates header.
        i. Reads header file from surface model: hdrgrid readhdrfile (char* thehdrfilename)
            1. Opens the hdr file (location specified in main function)
            2. Reads the header file (.ncols, .nrows, .ndv, .xll, .yll, .ncells, .cellsize)
            3. Determines the number of cells in the file
            4. Prints the header values for the user
            5. Closes the hdr file
        ii. Stores each value as header.XXXX from step 2
    c. Reads the float file: float* readfltgrid (char* thefilename, unsigned long int &nvalues)
        i. Opens the binary float file (location specified in main function)
        ii. Determines the file size
        iii. Allocates memory to store the entire file
        iv. Copies the file into buffer
            1. Prints the number of values in the file
            2. Prints the size of the file
            3. Prints the results
        v. Closes the file
            1. Prints that the flt file was read
            2. Stores the file in the buffer
    d. Asks the user for the ht above the surface model, h
    e. Asks the user for the desired slice thickness, t
    f. Calculates the values for the minimum and maximum slice values above the surface model
    g. Prints the slice values
    h. Creates a file for the points within the slice
        i. Opens the binary file with the data points
        ii. Creates new binary file including hdr file for output

iii. Reads header file from original bov file determines offset.x, offset.y and offset.z.
    1. Without header file all offsets set to 0
    2. Writes offsets from original bov file to each of 3 tile header files
    3. Closes tile header files
    4. Displays offsets for the header files
iv. Reads in each data point 1 by 1
    1. Get the elevation of the surface model for each point location
    2. Calculates the ht above the surface model for each point
    3. Filters points to within slice limits
        a. Writes files within limits to binary file
        b. Counts the number of points in the file
    4. Counts the number of points outside the limits
v. Closes binary files
vi. Prints the number of points written to the file
vii. Prints the number of points outside the limits
viii. Deletes the points from memory

i. Repeats the above step h for second dataset
j. Prints Slice Complete!

3. Tree finder, Requires: bov file from the slice for survey 1 and 2
    a. Welcome to the Tree Finder
    b. Asks the user for the typical tree diameter for the area.
    c. Calculates the cell size equal to the radius of the typical tree.
        i. Stores the value as cellsize
    d. Prints the cell size.
    e. Reads the points from the first survey.
        i. Opens the bov file (location specified in main function)
            1. Reads in points 1 x 1
            2. Determines the extents of the points
        ii. Closes the .bov file
        iii. Opens the header file
            1. Determines the offsets for the file
        iv. Closes the hdr file
        v. Stores the points as Survey1
    f. Reads the points from the second survey
        i. Opens the bov file (location specified in main function)
            1. Reads in points 1 x 1
            2. Determines the extents of the points
        ii. Closes the .bov file
        iii. Opens the header file
            1. Determines the offsets for the file
        iv. Closes the hdr file
        v. Stores the points as Survey2
    g. Creates the hash table for the first survey (uses Survey1 and cellsize)
        i. Determines the number of divisions in the dataset based on the extents in the x and y directions and the cellsize
        ii. Creates grid squares based on the number of divisions to cover the entire dataset
        iii. Reads in the points from the dataset 1 x 1 and places in the appropriate grid.
    h. Creates the hash table for the second survey (uses Survey2 and cellsize)
        i. Determines the number of divisions in the dataset based on the extents in the x and y directions and the cellsize

ii. Creates grid squares based on the number of divisions to cover the entire dataset
iii. Reads in the points from the dataset 1 x 1 and places in the appropriate grid.

i. Opens the file to write the tree locations from survey 1 to.
    i. Opens the text file from user specified location or creates the file if it does not already exist.
j. Opens the file to write the tree locations from survey 2 to.
    i. Opens the text file from user specified location or creates the file if it does not already exist.
k. Determines the tree location
    i. Looks at the dataset in blocks of 9 grids at a time (1 grid and the 8 grids next to it)
        1. Adds the x coordinates for each point in the block of 9
        2. Adds the y coordinates for each point in the block of 9
        3. Creates a temporary dataset of all the points in the block of 9
        4. Fits a circle to the points if there are more than 50 points in the block of 9 (Circlecreator)
            a. Reads in the temporary dataset
            b. Determines a circle for all points
                i. Calculates the mean of the x and y coordinates
                ii. Transforms x and y to local coordinate system by subtracting x and y from the mean of respective coordinate.
                iii. Calculates the summations of the u and v coordinates
                iv. Fills matrices to determine circle from all points using the summations
                v. Solves the matrix equation for a circle using linear algebra
                vi. Calculates the radius

vii. Transforms center of circle back to x and y coordinates

c. Using a threshold of 2 times the RMS filters points (Reiterative step)

i. Determines the distance each point is from the center of the circle

ii. If the distance is less than the radius + the threshold or greater than the radius - the threshold the point is used

iii. The usable points create a new dataset

1. If the new dataset has more than 70 points a new circle is fit in the same way as b above.
2. Results with x, y, z, radius and number of points used for the circle.

ii. Ends when the entire dataset is looked at.

l. Closes the files the tree locations were written to.

m. Prints Tree Finder Complete!

4. Movement, Requires: txt file from the trees determined by tree finder for survey 1 and 2
    a. Welcome!!
    b. Displays the file for each of the txt files.
    c. Displays “Working”
    d. Reads in the txt files.
        i. Opens the txt files (location specified in main function)
            1. Reads in tree locations 1 x 1
            2. Stores each tree location in memory
        ii. Opens a new txt file to write the movement to.
            1. Writes the first line of the txt file as a header
        iii. Opens the header file
            1. Determines the offsets for the file
        iv. Determines the closest trees between datasets
            1. Looks for trees with displacement if:
                a. Δr is less than or equal to 5 cm
                b. The trees from the Survey2 are within $\pm$ 1 grid cell
        v. Prints the both trees and movement for trees with
            1. Radius greater than 7 cm
            2. Radius less than 40 cm
            3. Circle RMS less than or equal to 5 cm (user defined)
        vi. Closes all 3 files
    e. Displays “Movement complete!”

APPENDIX B – ELECTRONIC APPENDIX TO C++ CODE